ISSN 0869-5911, Petrology, 2006, Vol. 14, No. 2, pp. 117–153. © Pleiades Publishing, Inc., 2006.
Original Russian Text © L.L. Perchuk, T.V. Gerya, D.D. van Reenen, C. A. Smit, 2006, published in Petrologiya, 2006, Vol. 14, No. 2, pp. 131–167.

P–T Paths and Problems of High-Temperature Polymetamorphism

L. L. Perchuk*, **, *, T. V. Gerya**, D. D. van Reenen***, and C. A. Smit*****

** Geological Faculty, Moscow State University, Vorob'evy gory, Moscow, 119899 Russia*
e-mail: llp@geol.msu.ru

*** Institute of Experimental Mineralogy, Russian Academy of Sciences, Chernogolovka, Moscow oblast, 142432 Russia*
e-mail: taras@iem.ac.ru

**** Department of Geology, University of Johannesburg, Aukland Park, Johannesburg, P.O. Box 524 South Africa*
e-mail: ddvr@na.rau.ac.za

Received November 30, 2004

Abstract—Many Precambrian granulite-facies metamorphic complexes contain so-called straight gneisses, which are massive rocks with a clearly pronounced blastomylonitic texture, lineation, and gneissosity. These rocks occur exclusively in high-temperature ductile shear zones, which can develop either during the primary exhumation of rock complexes or during the overprinting by high-temperature dynamometamorphism. The main criterion for distinguishing between these two types of straight gneisses is the configuration of their *P–T* trajectories, which are recorded in the mineral assemblages in these rocks and their host gneisses. Ductile shear zones developed in Archean granulite gneisses simultaneously with their exhumation, and, hence, their *P–T* trajectories are segments of decompression and/or isobaric cooling paths. Straight gneisses in Proterozoic polymetamorphic complexes commonly compose high-temperature ductile shear zones overprinted on Archean granulite complexes, and the *P–T* paths of these rocks are Z-shaped. This means that, at a constant pressure in the middle part of the continental crust, the T_{min} of the older *P–T* trajectory corresponded to T_{max} of the younger trajectory, and often $T_{max} - T_{min} > 100$°C. Such ductile shear zones commonly have a strike-slip morphology and can be easily seen in aerial photographs and discerned during structural geological surveying. These zones can overprint older gneisses without any notable thermal effect on the latter. Relations of this type were identified in the granulite complexes of Limpopo in South Africa, Sharyzhalgai in the southwestern Baikal area, and Lapland in the Kola Peninsula. The results of our research propose a solution for the well-known problem of the significant discrepancies between the isotopic ages in high-temperature–high-pressure complexes and the partial or complete distortion of radiogenic isotopic systems under the effect of a newly inflowing metamorphic fluid. The application of geochronologic techniques to these situations is senseless, and only *P–T* trajectories provide insight into the actual age relations between the discrete tectono-metamorphic stages. It is thus expedient to conduct not only structural studies of metamorphic complexes but also their detailed petrological examination and the calculation of their *P–T* paths before geochronologic dating.

DOI: 10.1134/S0869591106020019

INTRODUCTION

The late 20th and early 21st centuries were marked by the active studying of the composition and characteristics of high-temperature (HT) and high-pressure (HP) metamorphic complexes composing deep crustal zones. This research was conducted along the following major avenues:

—examination of the lithosphere by geophysical techniques (seismic tomography, gravimetry, measurements of the electric conductivity, thermal fields, etc.), which provide for new interpretations of the state of the lower crust and underlying continental lithosphere (see, for example, James *et al.*, 2001; Nguiri *et al.*, 2001);

—studying of the structure and composition of the lower crust by geological methods in areas where lower crustal rocks (deep-seated Precambrian granulite complexes and Phanerozoic gneiss complexes) are exposed at the surface or occur as nodules in kimberlite pipes (see, for example, Spetsius and Serenko, 1990; Koreshkova *et al.*, 2001; Dawson *et al.*, 1997);

—the development of methods enabling the calculation of the *P–T* trajectories of HT–HP complexes (see, for example, Perchuk, 1985, 1989, 2005; Perchuk *et al.*, 1996; Smit *et al.*, 2001; van Reenen *et al.*, 2004);

—isotopic dating of garnet, Al silicates, and other rock-forming minerals participating in metamorphic reactions (i.e., methods alternative to isotopic zircon dating; see, for example, Holzer *et al.*, 1998; Kreissig *et al.*, 2001; Boshoff *et al.*, 2004), techniques that provide (in spite of significant methodical difficulties) bril-

liant possibilities for the dating of these mineral reactions;

—numerical simulations of the dynamics of metamorphic complexes (see, for example, Gerya *et al.*, 2000), which made it possible not only to settle the seemingly insoluble problem of the exhumation of ultrahigh-pressure complexes (see, for example, Schreyer, 1988) but also to evaluate the velocities of their displacements in the crust and lithosphere (see, for example, A.L. Perchuk, 2003; A.L. Perchuk *et al.*, 1998; Gerya and Stoekhert, 2002; Gerya *et al.*, 2002), which were determined to have occasionally reached amazingly high values (Baldwin *et al.*, 2004; Camacho *et al.*, 2005).

In spite of the progress in metamorphic petrology, structural geological studies have remained at a practically unchanged level, and several researchers still try to identify multiple deformation stages and then correlate them with geochronological data, ambiguous *P–T* paths, and speculative geodynamics (see, for example, Aftalion *et al.*, 1991; Treloar *et al.*, 1992; Stevens *et al.*, 1997; Holzer *et al.*, 1998; Schaller *et al.*, 1999). This often results in misunderstanding and hampers geological surveying. This phenomenon stems from the overcomplicated interpretation of relatively simple phenomena and processes, whose kernel is far from always obvious. One of such processes is *high-temperature polymetamorphism* and its unusual geological manifestations, which are discussed in this paper. Polycyclic high-temperature metamorphism has been known for a long time, but it is still quite difficult to identify its geological manifestations. Because of this, before proceeding to the analysis of this process, let us define some terms that will be used below. *Polymetamorphism* is the overprinting of younger mineral assemblages onto older ones in the course of a single geodynamic event (see, for example, *Metamorphic Zoning…*, 1983; Fonarev *et al.*, 1998). Reliable indications of this phenomenon are the development of principally new mineral assemblages (such as high-pressure eclogitization of metabasites), reaction textures (for example, the development of coronites), and the chemical zoning in mineral grains. The time gaps between metamorphic events can vary in discrete complexes from a few million to hundreds of million years. This phenomenon is described by thoroughly elaborated techniques for the calculation of *P–T* paths. *Diaphthoresis* is repeated metamorphism related to the onset of another geodynamic event, which can occur millions of years to hundreds of million years after the preceding metamorphic event. In Precambrian granulite complexes (as well as in ultrahigh-pressure complexes), diaphthoresis is usually thought to have resulted in the development of lower temperature mineral assemblages after higher temperature associations (see, for example, Korikovsky, 1967; Fonarev, 2003). However, this process is not always associated with the hydration of minerals. For instance, mafic and ultramafic rocks in deep ductile shear zones are transformed into eclogites and garnet peridotites under the effect of water-rich fluid. This process was first studied by Udovkina (1972) in the Polar Urals and was later justified experimentally and petrologically for the Norwegian Caledonides that developed after Precambrian metabasites (see, for example, Austrheim and Griffin, 1985; Austrheim, 1990).

It is known that the mineral assemblages of granulites can very rarely preserve a record of the prograde and even culmination metamorphism (see, for example, Perchuk *et al.*, 1985; Zeh *et al.*, 2004) because of the very intense deformational and high-temperature regimes of the prograde metamorphism. However, virtually all deep-seated complexes contain massive rocks with clearly pronounced linear gneissosity and blastomylonitic textures. These rocks also often grade into augen gneisses. They compose *ductile shear zones* or zones of dynamometamorphism, i.e., "juvenile" metamorphism that not always can be identified in field. These rocks commonly display no traces of infiltration metasomatism, a fact that makes it possible to use the mineral assemblages of these rocks to evaluate the temperatures and pressures and calculate the *P–T* trajectories (see, for example, van Reenen *et al.*, 2004). This does not rule out the possibility of the later hydrothermal alterations in high-temperature dynamometamorphic zones in the upper crust up to the development of typical mylonites (see, for example, Smit *et al.*, 2001). The latter are usually produced with the transition between ductile and brittle deformations (see, for example, Passchier and Trouw, 1996). To clarify the term *zones of high-temperature dynamometamorphism*, it is expedient to recall the history of their discovery.

Zones of HT–HP dynamometamorphism were first documented and exhaustively examined in metabasites of the southwestern Grenville province in the Canadian Shield (Davidson, 1984a, 1984b; Bush *et al.*, 1995) and, later, in the Limpopo granulite complex (Smit and van Reenen, 1997). The rocks composing these complexes were named *straight gneisses*, and this term will be used in this publication as one not having any classic analogues. Since these rocks have blastomylonitic textures, they are sometimes referred to as mylonites (see, for example, Smit *et al.*, 2001). This term itself was, however, repeatedly criticized because it was originally applied to the products of brittle deformations that are produced in zones of rock shattering at low temperatures. Analogues of straight gneisses are known among mica schists, which are nodular, strongly sheared rocks with large porphyroblasts of garnet, kyanite, and, more rarely, staurolite (Davidson, 1984). These rocks often contain garnet with snowball structures (see, for example, Perchuk and Krotov, 1998 and references therein).

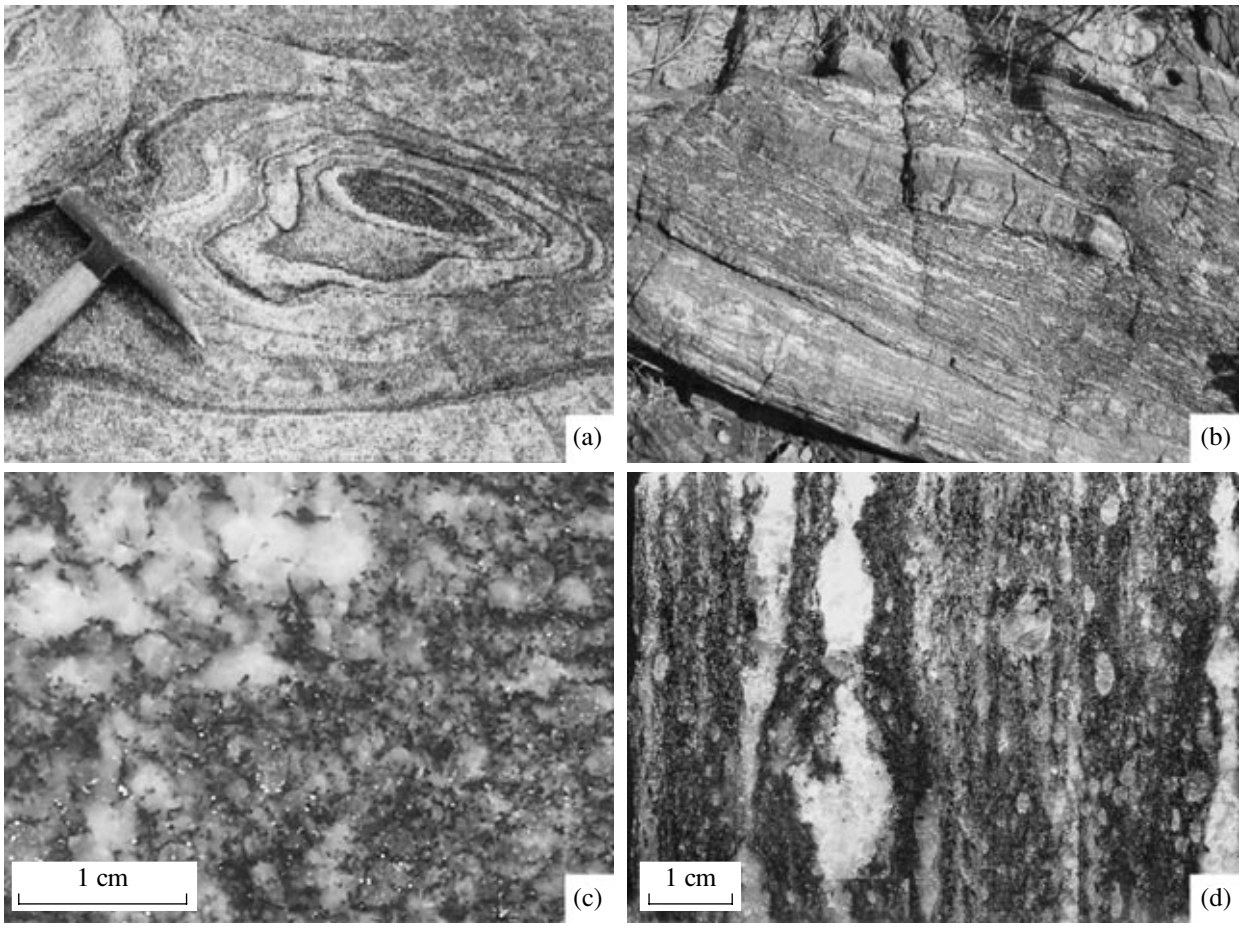

Fig. 1. Macrotextural features of the transformation of normal *Bt-Grt-Crd* gneisses into straight gneisses of the same mineral composition under granulite-facies conditions (Central Zone of the Limpopo granulite complex). (a) Small equant fold in normal gneisses (perhaps, D2/M2); (b) boudin of an equant fold (D2/M2) that originally resembled the fold in Fig. 1a and was then deformed and transformed into a boudin during overprinted high-temperature dynamometamorphism (D3/M3); (c) macrotexture of normal gneiss (D2/M2) with well pronounced plication and crenulation of its leucosome, which are typical traces of the buoyant ascent of a rock (Gerya *et al.*, 2000) in a relatively low-viscosity ($\eta \le 10^{19}$ Pa s) medium; (d) typical macrotexture of straight gneiss (D3/M3).

These schists are formed in medium-temperature shear zones (zones of ductile deformations), in which high plasticity of the rocks is reached during deformations because of the abundance of layer silicates (biotite, muscovite, and chlorite). Granulite-facies straight gneisses are different: these are strongly sheared rocks with a pronounced schistose structure and a blastomylonitic texture. They differ from adjacent coeval ortho- and paragneisses. The "normal" gneisses also have schistose structures, but they are extensively plicated, display crenulated banding, and bear ptigmatites (Fig. 1c), i.e., textural features that have never been found in straight gneisses. These elements disappear from rocks in deep-seated zones of granulite-facies dynamometamorphism. The gneisses acquire a linear orientation of all of their planar elements (foliation), the folds become stretched and broken, and the ptigmatites are linearly deformed. Small sheath folds (Fig. 1a) are transformed into zonal boudins (Fig. 1b). The fragmented leucosome (ribbon structure) acquires clear lineation (Fig. 1d). The distribution of fine-grained lens-shaped aggregates of mafic minerals shows parallelism (stretching lineation). The latter two features make it possible to identify the transport direction in the rock (see, for example, Passchier and Trouw, 1996; Smit and van Reenen, 1997; Smit *et al.*, 2001). Straight gneisses equally frequently develop in quartz-bearing and quartz-free rocks.

In Precambrian granulite complexes, high-temperature assemblages often overprint lower temperature associations. At the first glance, this process is chaotic, but, in fact, the detailed interpretation of aerial photographs and the results of structural geological mapping reveal that straight gneisses are spatially restricted to multiple zones of high-temperature ductile deformations (dynamometamorphism). For example, these rocks in the Central Zone of the Limpopo Complex compose numerous linear and *en-echelon* zones of vari-

able thickness, which are overprinted on all older metamorphic rocks, including the straight gneisses that were produced synchronously with the exhumation of the complexes from the lower crust. For example, straight gneisses generated during exhumation can contain a newly formed generation of garnet Grt_1, which is, in turn, replaced by garnet of younger generation, Grt_2, during a much later metamorphic event.[1] The rocks are sometimes completely recrystallized with the development of newly formed higher temperature assemblages, which are, in turn, affected by polycyclic high-temperature metamorphism. This process generates flattened garnet grains with the growth of reaction textures only on one side of them (van Reenen *et al.*, 2004). These straight gneisses can be tens to hundreds of million years younger than the surrounding rocks (see, for example, Boshoff *et al.*, 2004). A glaring example of this phenomenon is provided by the polymetamorphic rocks of the granulite core of the Vredefort crater. The local granulite-facies medium-depth rocks have average age of ~3.1 Ga (Hart *et al.*, 1999, 2004) and were overprinted by mineralogically analogous but higher temperature mineral associations with an age of ~2 Ga (see, for example, Perchuk *et al.*, 2002 and references therein).

Thus, Archean lower crustal complex can include dynamometamorphic zones that facilitate the uplift of rocks to higher continental crustal levels or the exhumation of these rocks (deformation–metamorphic stage D2/M2). In polymetamorphic complexes, zones of high-temperature dynamometamorphism (deformation–metamorphic stage D3/M3) overprint granulite-facies rocks that were produced during older evolutionary stages of the continental crust. The rocks of D2 and D3 practically cannot be distinguished without thorough structural examination and can be identified only by the detailed petrological study with the calculation of their *P–T* paths. However, accurate information on the actual age of these rocks can be obtained only with the use of an expensive complex isotopic research. Note that the first deformation stage D1 is always related to the tectono-metamorphic transformation of the protoliths before their subsidence to significant depths (for example, these can be the rocks of greenstone belts). Theoretically, the number of deformation stages can be arbitrary great, but here we limit ourselves to the consideration of D2 and D3, because information on them is the most abundant.

METHODS APPLIED TO STUDYING DEEP DYNAMOMETAMORPHIC ZONES IN PRECAMBRIAN GRANULITES

Detailed petrological investigations in deep dynamometamorphic zones in HP–HT complexes and their outer contacts (Bush *et al.*, 1995; Smit *et al.*, 2001) have revealed the mechanisms responsible for their origin and preservation during deep metamorphism. For example, it was demonstrated (Perchuk and Gerya, 2004; Perchuk *et al.*, 1996, 2001a) that the Archean exhumation of several granulite complexes proceeded not according to the mechanism of simple gravitational redistribution within the scope of the viscous liquid model (see, for example, Gerya *et al.*, 2000) but in the form of vast blocks. When "floating" to the surface [the term was coined by Korzhinskii (1999, p. 141)], these blocks "slide" along the separating zones of low relative viscosity similarly to ice blocks in rivers or to mudflows. It cannot be ruled out that the decrease in the rock viscosity in D2 zones results from fluid filtration along these zones, but this fluid does not exert any significant hydrothermal–metasomatic effect on the mineral assemblages. Traces of such ductile shear zones are left in the form of D2 straight gneisses. As was mentioned above, these rocks are coeval with the granulites of the ascending blocks but preserve record only of the youngest metamorphic reactions (the lowermost segments of the *P–T* paths; Perchuk *et al.*, 1996). Simultaneously with exhumation, *Ky-Ms-Bt-St-Chl* schists "circulate" in the ductile shear zones between the granulites and craton rocks, a process recorded in mineral equilibria in the form of *P–T* loops (see, for example, Perchuk and Krotov, 1998; Perchuk *et al.*, 2001a).

Thus, thank to ductile deformations, normal granoblastic D2 gneisses (Figs. 1a, 1c) in the middle crust can be transformed into D3 straight gneisses with blastomylonitic textures (Figs. 1b, 1d). This process is coupled with the origin of principally different mineral assemblages (M3) that bear no traces of any significant mineral reequilibration in M2 assemblages.

Below we will discuss the specifics of these processes during deep-seated metamorphism and exhumation of granulite complexes and characterize the typical manifestations of dynamometamorphic zones during stages D2/M2 and D3/M3 to facilitate the elaboration

[1] Notation: **Minerals:** *Alm*—almandine, *And*—andalusite, *Andr*—andradite, *Ap*—apatite, *Bt*—biotite, *Chl*—chlorite, *Cpx*—clinopyroxene, *Crd*—cordierite, *Cum*—cummingtonite, *Ilm*—ilmenite, *Grs*—grossular, *Grt*—garnet, *Hbl*—hornblende, *Kfs*—potassic feldspar, *Ky*—kyanite, *Mag*—magnetite, *Ms*—muscovite, *Opx*—orthopyroxene, *OK*—"orthocorundum" ($AlAlO_3$), *Qtz*—quartz, *Pl*—plagioclase, *Prp*—pyrope, *Rt*—rutile, *Sil*—sillimanite, *Spl*—spinel, *Spr*—sapphirine, *St*—staurolite, *Zrn*—zircon. **Expression for mole fractions of components in minerals:** $X_{Mg}^{Grt} = Mg/(Mg + Fe + Mn)$, $X_{Ca}^{Grt} = Ca/(Ca + Mg + Fe + Mn)$, $X_{Mg}^{Opx} = Mg/(Mg + Fe + Mn)$, $X_{OK}^{Opx} = 0.5Al/(0.5Al + Fe + Mg)$, $X_{Mg}^{Bt} = Mg/(Mg + Fe + Mn)$, $X_{Mg}^{Crd} = Mg/(Mg + Fe + Mn)$, $X_{Mn}^{Grt} = Mn/(Mg + Fe + Mn)$, $N_i^{Min} = 100X_i$ is the molar percentage of component i in mineral (*Min*). $a_{H_2O}^{fl}$ is the water activity in fluid (*fl*).

of criteria for their distinguishing (both in field and in the laboratory) for the purposes of geochronologic research. One of the main criteria is the configuration of the *P–T* trajectories (Perchuk, 2005).

Although the first *P–T* paths were calculated more than thirty years ago (see, for example, Perchuk, 1973, 1976, 1977, 1989), discussions about the techniques for their derivation continued until recently (see, for example, Frost and Chacko, 1989; Spear and Florence, 1992; Spear, 1993; Gerya *et al.*, 2000; Smit *et al.*, 2001; van Reenen *et al.*, 2004). Since *P–T* trajectories are considered in this paper to be indicators of high-temperature polymetamorphism, it is pertinent to remind the methods of their derivation that have became conventional and find wide application to studying complexes of various metamorphic facies (see, for example, Smit *et al.*, 2001; Gerya and Maresch, 2004; van Reenen *et al.*, 2004; Hisada *et al.*, 2005).

(1) Structural geological research. Since metamorphism is always coupled with rock deformations, and each metamorphic stage corresponds to a stage of deformations, geochronologic studies of metamorphic complexes are always associated with their structural geological examination. However, lately these techniques seem to have come to a standstill in application to metamorphic complexes: various researchers sometimes manage to distinguish different numbers of metamorphic and deformational stages, cycles, etc. (sometimes, dozens of them; see, for example, Aftalion *et al.*, 1991). There are still no indicators of the high-temperature repeated metamorphism (D3) of high-pressure rocks metamorphosed to the granulite and eclogite metamorphic facies. The results of our preliminary research have demonstrated that the origin of D3 ductile shear zones is directly related to high-temperature repeated metamorphism.

Figures 1a and 1b display how a concentrically zoned boudin could develop from a sheath fold (Fig. 1b), which was produced, according to geological evidence, in the Archean (D1 or D2), and repeated metamorphism was overprinted onto the primary texture of the rock some 600 m.y. later (M3). Recall that the first metamorphic event M1 was related to the origin of the gray gneiss complex in the Kaapvaal craton (the protolith of the D2/M2 and D3/M3 gneisses) at 3.34 Ga (Hofmann *et al.*, 1998; Kröner *et al.*, 1999). The textures of the rocks (Figs. 1c, 1d) also provide evidence of two deformational events: one of them resulted in normal migmatized gneiss (Fig. 1c), and the other ended with the origin of straight gneiss (Fig. 1d). It is impossible to visually determine whether these events were synchronous or not. These are a few of multiple examples, and much of this information can be obtained exclusively by geological structural mapping with the application of conventional techniques for revealing the spatial distribution of planar and linear features of crystalline rocks (filed measurements and their stereographic interpretations).

(2) *P–T* trajectories. The rule "one metamorphic cycle—one *P–T* path" (see, for example, Perchuk, 1976, 1985; Harley, 1989) becomes senseless in application to high-temperature dynamometamorphism: the same complex can be characterized by various *P–T* trajectories (Perchuk *et al.*, 2001b). Their calculation is not obvious. There are several thermodynamic databases (for example, Holland and Powell, 1998; Gerya *et al.*, 2004; Gerya and Perchuk, 1997) and approaches (see, for example, *Metamorphic Zoning…*, 1983; Smit *et al.*, 2001; Gerya *et al.*, 2004). In this publication we make use of the recently improved technique (Smit *et al.*, 2001; van Reenen *et al.*, 2004), whose core is briefly characterized below.

Samples. The stone material is sampled in an exposure that has been thoroughly examined by structural geological methods and is correlated to a certain type of deformations.

Petrostructural analysis. The aim of these investigations is to reveal the crystallization succession of minerals and the development of reaction textures in thin sections.

Microprobe analyses are conducted to identify the trends in the compositional evolution of minerals participating in exchange (continuous) and net-transfer (discontinuous) reactions. The most efficient technique is the detailed microprobe profiling of the largest grains of these minerals (these are often porphyroblasts) of variable composition in order (a) to reproduce the flat profile of chemical zoning in the cores of the grains with N_{Mg} = max (metamorphic culmination) and (b) to determine the number of generations produced during younger metamorphic stages.

Geothermobarometric calculations. All of such calculations are conducted based on the results obtained on mineral equilibria in metapelites. It should be explained why these rocks are selected as indicators of mineral-forming processes during metamorphism, because lately some ambitious researchers with limited knowledge of Korzhinskii's principle of local equilibrium cast doubt on the utilization of metapelites for evaluating the parameters of mineral equilibria and calculating *P–T* paths (*Metamorphic zoning…*, 1983). It became clear already in the 1970s that metapelites are the most reliable indicators of the metamorphic regimes of almost all metamorphic facies (see, for example, Korikovsky, 1979; Perchuk, 1973). These rocks can be found in any metamorphic complex around the world. Moreover, many metapelites possess well developed reaction textures, which enable the researcher to fully utilize the simplest calculations in the Al_2O_3–FeO–MgO system to evaluate the *P–T*-

$a^{fl}_{H_2O}$ parameters of the metamorphic processes and elucidate the evolutionary history of these complexes. Because of this, exchange mineral reactions most common in metapelites were selected for this purpose in the 1970s–1980s, including

$$Grt_{Fe} + Crd_{Mg} = Grt_{Mg} + Crd_{Fe} \quad (1)$$

$$Grt_{Fe} + Bt_{Mg} = Grt_{Mg} + Bt_{Fe} \quad (2)$$

$$Grt_{Fe} + Opx_{Mg} = Grt_{Mg} + Opx_{Fe}, \quad (3)$$

which can be successfully used as mineral thermometers (Aranovich, 1991; *Biotite–Garnet–Cordierite Equilibria…*, 1983; Harley, 1984; Perchuk and Lavrent'eva, 1983, 1990), as well as the equilibria

$$Crd = Opx_{Al} + Qtz \quad (4)$$

$$Grt + Qtz = Crd + Opx \quad (5)$$

$$Grt + Sil + Qtz = Crd, \quad (6)$$

which are applied as mineralogical barometers (Aranovich and Kosyakova, 1984; Aranovich and Podlesskii, 1989; Perchuk *et al.*, 1985). These investigations made it possible to build a thermodynamically consistent database (see, for example, Perchuk *et al.*, 1985) and the GEOPATH software package (Gerya *et al.*, 2004; Gerya and Perchuk, 1990, 1992) for thermodynamic calculations. Equilibria in the system $MgO–FeO–Al_2O_3–K_2O–H_2O$ thus became benchmarks for all complexes for which local equilibrium conditions were determined using the same methods. The temperatures are commonly calculated based on the compositions of the margins and cores of grains of Fe–Mg minerals (for example, core–core and margin–margin). For this purpose, it is necessary to find (in a thin section) a flat chemical profile through the cores of equilibrium phases with the highest X_{Mg}. In utilizing discontinuous equilibria for the evaluation of the pressure and/or $a^{fl}_{H_2O} = f(T)$, the researcher should avoid making use of the compositions of the outermost parts of mineral grains with pronounced diffusion-controlled zoning, which develops as a consequence of diffusion exchange during the latest cooling stages of the rock, when discontinuous reactions cease to proceed. When reactions with cordierite are utilized, one should calculate the dependence $a^{fl}_{H_2O} = f(T)$ from any hydration–dehydration reaction, first of all, by the reaction

$$Grt + Kfs + H_2O = Bt + Sil + Qtz. \quad (7)$$

Calculation of P–T trajectories. The reader can find detailed descriptions of the successive operations used to calculate *P–T* paths in our earlier publications (*Metamorphic Zoning…*, 1983; Korikovsky and Perchuk, 1983; Perchuk *et al.*, 1996; Perchuk, 1985; Smit *et al.*, 2001; van Reenen *et al.*, 2004). Note that these trajectories should be derived by calculating the thermodynamic parameters of local equilibria, and one should systematically check the consistency of the paths with the compositional isopleths of minerals of variable composition in *P–T* diagrams. Preparatory, the petrography of the thin sections should be thoroughly examined and described in order to identify the succession of mineral reactions. For example, the reaction of decompressional cooling *Grt* + *Qtz* = *Opx* + *Crd* (5) can give way to the reaction of subisobaric cooling *Crd* ⇒ *Grt* + *Sil* + *Qtz* (see, for example, Perchuk *et al.*, 1996; Gerya and Maresch, 2004).

Fluid inclusions. Using an accurate approach to studying fluid inclusions in minerals, the researcher can obtain amazingly accurate and exact information not only on the composition of the locally equilibrated fluid but also on the *P–T* parameters of its capturing (see, for example, Tomilenko and Chupin, 1983; Berdnikov, 1987; Touret, 2001; Touret and Hartel, 1990). If a rock sample contains fluid inclusions, the *P–T* trend can be obtained for this rock without utilizing mineralogical barometry. For this purpose, data on the densities of these inclusions are used in combination with pressure-independent mineralogical thermometers (Perchuk, 1987, 1989). The theoretical basis of this approach is obvious enough: metamorphic reactions proceed not only simultaneously with deformations but also in the presence of a fluid. Hence, minerals occur in equilibrium with fluids differing in density and composition during each metamorphic stage. Inasmuch as minerals recrystallize and capture fluid during exhumation, this fluid is always in local equilibrium with the host mineral grain. There is the possibility of determining the composition and other characteristics of this fluid using its inclusions in minerals (Smit and van Reenen, 1997; Hisada *et al.*, 2005) and also by the direct thermodynamic calculations of $a^{fl}_{H_2O}$ from the equilibria *Grt* + *Kfs* + H_2O = *Bt* + *Sil* + *Qtz* (Aranovich, 1991; Perchuk, 1987, 1989) by the GEOPATH computer package (Gerya and Perchuk, 1994).

Changes in the modal composition of rocks. Discontinuous reactions modify the qualitative mineral proportions (modes). For example, the amount of garnet in bivariant equilibria diminishes during the decompressional cooling of metapelites and increases during isobaric cooling. One can plot the derived *P–T* trajectory in a diagram with equal concentrations of garnet in the rock and check whether this trajectory matches such relations. For this purpose, the researcher has to have only a chemical analysis of the rock and the *P–T* coordinates of the trajectory (see, for example, Gerya, 1999; Gerya and Maresch, 2004; Smit *et al.*, 2001). One can also utilize polymineralic modes (Carson *et al.*, 1999; Wei *et al.*, 2003) and the THERMOCALC computer program (Holland and Powell, 1998).

Numerical test. Whenever possible, the *P–T* paths should be tested by means of numerical simulations (see, for example, Gerya *et al.*, 2000, 2002). A coincidence between the *P–T* path deduced from natural mineral assemblages of the rocks and the trajectory simu-

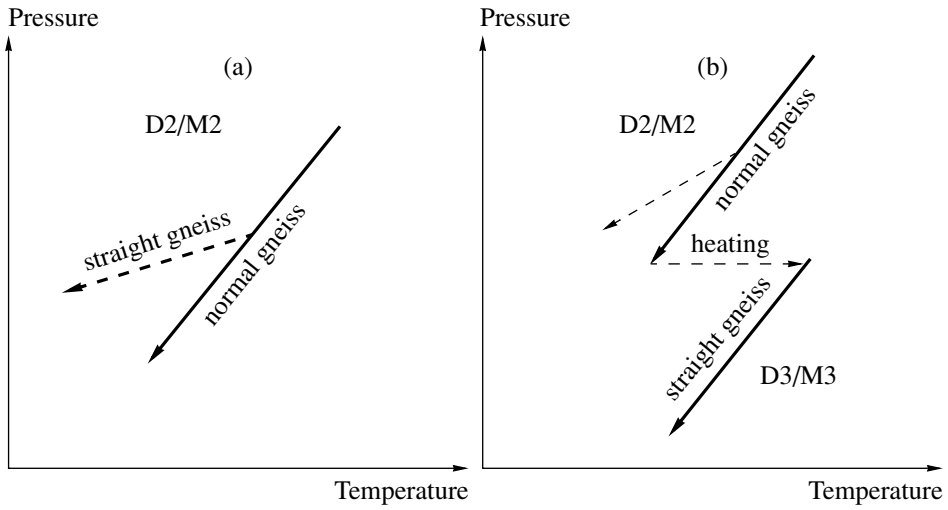

Fig. 2. Schematic representation of various types of *P–T* trajectories for (a) decompressional cooling of the rocks in the course of their exhumation toward the surface (D2/M2) and (b) high-temperature dynamometamorphism (D3/M3), whose mineral assemblages are overprinted onto the assemblages of earlier metamorphic events (Perchuk, 2005).

lated using the densities and rheological characteristics of these rocks provides additional argument in support of the plausibility of the path.

If all of the aforementioned conditions are fulfilled, the researcher receives a convincing argument that the derived *P–T* trajectory is accurate enough and requires only its realistic and accurate geological and geodynamic interpreting.

The *P–T* paths of straight gneisses from D2 zones coincide with the paths of normal gneisses that were exhumed in blocks simultaneously with the development of D2 ductile shear zones. However, the *P-T* trajectories of normal gneisses are "cut off" due to the obliteration of the high-temperature record from the mineral equilibria and, thus, display a clearly pronounced segment of isobaric cooling (Perchuk *et al.*, 2001a; Smit *et al.*, 2001). Conversely, the *P–T* trajectories of straight gneisses from D2 zones occur to be both lower pressure and higher temperature (van Reenen *et al.*, 2004). Figure 2 schematically exhibits the differences between the *P–T* trajectories for D2 complexes (Fig. 2a) and D3 zones of high-temperature dynamometamorphism (Fig. 2b). As was already mentioned above, a noteworthy example of a D3 record is offered by granulite-facies metapelites in the core of the Vredefort impact crater. These rocks display clearly pronounced evidence of repeated high-temperature metamorphism, which was induced by rock heating and uplift under the effect of the shock wave (Perchuk *et al.*, 2002). Figure 3 demonstrates a *P–T* diagram that clearly defines the D2 stage of regional metamorphism (~3.1 Ga; Hart *et al.*, 1999, 2004; Moser *et al.*, 2001) and the postimpact D3/M3 stage (~2 Ga; Armstrong *et al.*, 1991; Kamo *et al.*, 1996). The *P–T* evolution of the Vredefort dome (Fig. 3) is thought to be a model for the development of dynamometamorphism in ductile shear zones in granulites.

(3) Fluid regime of dynamometamorphism. During the transition between ductile and brittle deformations in the course of the exhumation of HT–HP complexes, thick zones of hydrothermal alteration can develop in straight gneisses, which associates with the significant inflow and outflow of components. These zones have long been known, are widely spread in many granulite complexes, and will not be discussed in this publication. For example, relatively low-temperature infiltration-metasomatic rocks were studied and analyzed in the shear-zones of the Southern Marginal Zone of the Limpopo Complex (Smit and van Reenen, 1997; Smit *et al.*, 2001). At the same time, deformations, heating, and metamorphic reactions cannot occur in D3 zones without inflow of heat and aqueous fluids. Their abundance is apparent from the several generations of biotite and numerous tiny shear zones (no thicker than a few micrometers). Made up of biotite, sillimanite, and quartz (see, for example, van Reenen *et al.*, 2004), these zones are produced by high-temperature acid leaching (Korikovsky, 1967), i.e., by infiltration metasomatism. Such tiny shear zones can occur in many (if not all) granulite complexes, but they cannot be utilized for mineralogical barometry due to two reasons: (a) only rarely can it be established that the sillimanite was in equilibrium with the mafic minerals of matrix, and (b) the classic form of the Gibbs thermodynamic potential is inapplicable to systems with perfectly mobile components, because a minimum of this potential can be reached not only at constant *T* and *P*

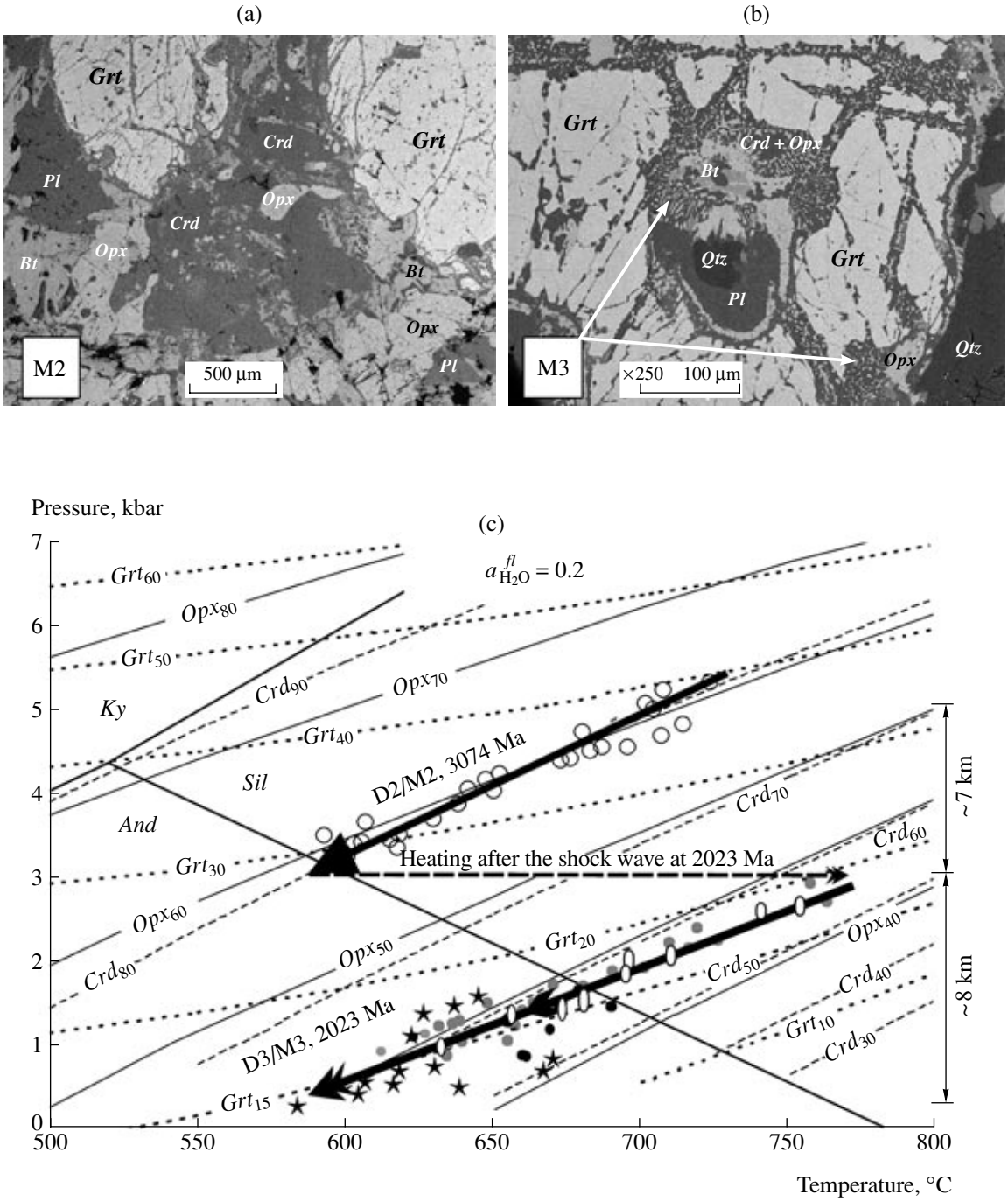

Fig. 3. Reaction textures *Grt* + *Qtz* ⇒ *Opx* + *Crd* in metapelites (D2/M2) in the core of the Vredefort crater that were affected by high-temperature metamorphism after the impact (D3/M3) and the *P–T* trajectories of their evolution (modified after Perchuk *et al.*, 2002). (a) Microtexture of granulite metapelite produced by regional metamorphism (M2) in the Archean; (b) reaction microtexture produced in the metapelite after the impact as a result of reaction between *Grt* and *Qtz*; (c) *P–T* trajectories for the prograde regional metamorphism (D2/M2) and overprinted high-temperature metamorphism (D3/M3) in the granulite. Metamorphic event D2/M2 corresponds in Fig. 3c to the stage of buoyant ascent of the granulite complex within the Kaapvaal craton at approximately 3.08 Ga (Hart *et al.*, 1999; Moser *et al.*, 2001). The *P–T* trajectory for D3/M3 is recorded in symplectites from pseudotachylite and implies their origin after the impact and heating, during the uplift of the central part of the dome at 2.023 Ga (Armstrong *et al.*, 1991; Kamo *et al.*, 1996). The *P–T* trajectory for the exhumation of granulites in the Archean (D2/M2) is marked by open circles. Open ellipses and gray and black circles mark the *P–T* trajectory for the development of symplectites during the D3/M3 stage (data obtained by the thermometry of the reaction textures in three samples). Asterisks mark the *P–T* parameters under which the ultramylonites were produced during the final ascent stages. All data, including the compositional isopleths for the *Grt* + *Qtz* = *Opx* + *Crd* equilibrium are recalculated to a water activity in the fluid equal to 0.2.

but also via the stabilization of the chemical potentials of the perfectly mobile components.

(4) Geochronology. Since *P–T* paths are derived for metamorphic complexes from reactions (1)–(7), this requires the isotopic dating of the metapelites. Zircon, a mineral considered to be a reliable geochronologic indicator, occurs, in fact, to be "useless" when high-temperature metamorphism should be dated. Furthermore, the application of the conventional isotopic dating of zircon and/or monazite from metapelites is often senseless: the multiple recrystallization of these minerals results in their unsystematic discordant age values. Because of this, it is practically impossible to correlate certain *P–T* trajectories with individual metamorphic events. The age of zircon from metapelites sometimes appears to differ by hundreds of million years or more from the age of mineral reactions participated by garnet (see, for example, Daly and Bogdanova, 1991; Holzer *et al.*, 1998; Boshoff *et al.*, 2004). Because of this, the evolution of polymetamorphic complexes can be examined using, along with zircon dating, the isotopic dating of minerals that are involved in the reactions (*Grt, Crd*, and *Sil*) on which the *P–T* trajectories are based.

Final conclusions concerning M3 metamorphism can often be drawn only by investigating reaction textures between minerals and by constructing *P–T* paths with subsequent geochronologic dating, whose results can not always be realistically interpreted because of the distortion of isotopic equilibria under the effect of even very weak high-temperature metamorphism. Below we consider some examples (which are still very scarce) of relations between D2 and D3 in ductile shear zones in some HT–HP metamorphic complexes.

HIGH-TEMPERATURE POLYMETAMORPHISM IN THE LIMPOPO GRANULITE COMPLEX

The Limpopo Complex was comprehensively characterized elsewhere (see, for example, van Reenen and Smit, 1996; Smit *et al.*, 2001; van Reenen *et al.*, 1990, 1992, 2004). It is pertinent to remind that the Limpopo Complex (300 × 700 km) in South Africa is a classic Archean granulite-facies gneiss terrane. It is situated between two cratons—Kaapvall in the south and Zimbabwe in the north (Fig. 4, inset)—and is subdivided into the Central, Southern Marginal, and Northern Marginal zones.

The *Northern Marginal Zone* (~2620 and 2580 Ma) is made up of a plutonic and supracrustal associations. The plutonic association is spread more widely and consists of charnockites and porphyritic granitoids that cut the supracrustal association. Large homogeneous charnockite bodies compose narrow thin extended sheets among tonalite gneisses. They consist of the primary *Pl + Opx + Qtz + Kfs + Bt* assemblage with subordinate amounts of *Cpx*, *Hbl*, and *Grt*. The porphyritic granites of the Razi suite are exposed along the boundary between the Northern Marginal Zone and the Zimbabwe craton (3.5–2.6 Ga) over a distance of about 100 km. The supracrustal association is composed of lithological analogues of greenstone rocks and accounts for approximately 10% of the Northern Marginal Zone by area. The predominant rock types are mafic granulites (*Qpx + Cpx + Pl + Hbl*), amphibolites, and magnetite quartzites. The metapelites typically have decompressional reaction textures, such as *Grt-Qtz-Sil* ⇒ *Crd*. High-temperature magnesian varieties consist of *Grt + Qtz + Sil + Crd* and *Opx*, but *Opx* and *Sil* have never been observed in physical contact.

The *Southern Marginal Zone* (2.69 Ga; Kreissig *et al.*, 2001) contains widespread tonalitic gneisses and metapelites of the Bandalierkop Formation, which also contains small bodies of metamorphosed basic and ultrabasic rocks and BIF. The gneisses are extensively deformed and migmatized. The metapelites consist of *Qtz*, *Pl*, *Opx*, *Grt*, *Bt*, and *Crd* and contain more rare perthitic *Kfs*, *Spl*, and *Sil*. These rocks are coarsely banded, often migmatized, and contain symplectitic reaction textures analogous to those in the aluminous rocks of the Central and Northern Marginal zones. The leucocratic constituent is dominated by perthitic *Kfs* and *Pl* with minor amounts of graphite, *Grt*, *Sil*, and *Crd*. The Southern Marginal Zone is separated from the Kaapvaal craton (3.34–3.08 Ga; see, for example, Hofmann *et al.*, 1998) by the Hout River shear zone, whose age was estimated at 2689 ± 7 Ma using synkinematic kyanite (Kreissig *et al.*, 2001). The Southern Marginal Zone is cut across by a system of sublatitudinal zones (~1 km thick) of ductile deformations that dip southward (Fig. 4). These zones were produced during uplift and the formation of granulites (Smit and van Reenen, 1997). The thick Palala shear zone (2 Ga, van Reenen and Smit, 1996) separates the Central Zone from the Southern Marginal Zone (Fig. 4). The metamorphic culmination in the latter was dated at 2691 ± 4 Ma on monazite from gneisses. This age corresponds to the age of the Hout River shear zone. The D2 ductile shear zones are coeval with the granulites and were produced during the exhumation of the complex (Smit and van Reenen, 1997; Smit *et al.*, 2001).

The *Central Zone* is characterized by widespread traces of polymetamorphism that was brought about by two major high-temperature events: one between ~2.63 and 2.57 Ga and the other at approximately 2 Ga. The zone is composed of metasediments and various orthogneisses with minor amounts of eulysites and boudined metabasites and metaultrabasites, which are high-temperature analogues of komatiites in greenstone belts adjacent to the Kaapvaal and Zimbabwe cratons. The most common rocks are normal tonalite gneisses with granoblastic textures, with straight

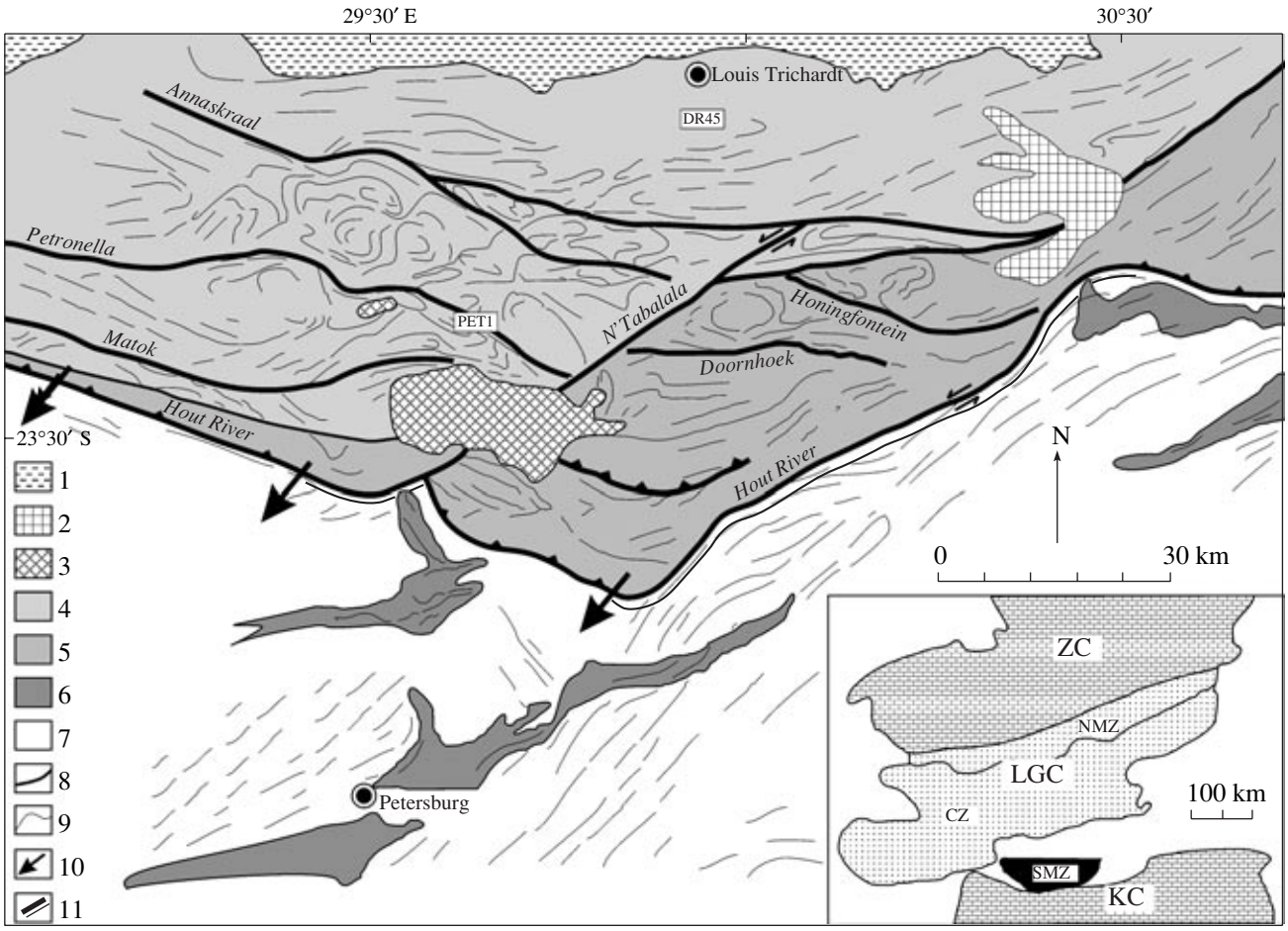

Fig. 4. Major dynamometamorphic zones of the Southern Marginal Zone in the Limpopo granulite complex, South Africa, and the adjacent northern part of the Kaapvaal craton (modified after Perchuk *et al.*, 1996).

(1) Sedimentary cover; (2) Schiel alkaline complex (1850 Ma); (3) Matok granite massif (2670 Ma); (4) granulites of the Southern Marginal Zone (2691 Ma); (5) zone of synchronous granulite hydration (van Reenen and Smit, 1996); (6) greenstone belts in the Kaapvaal craton; (7) Kaapvaal craton; (8) ductile shear (dynamometamorphic) zones in granulites, no more than a few hundred meters thick; (9) structural form lines; (10) direction of granulite exhumation (220° SW) determined from their lineation; (11) Hout River dynamometamorphism zone that separates the Southern Marginal Zone of the Limpopo granulite complex from the Kaapvaal craton. The map also shows the sampling sites of samples PET1 and DR45.

The inset displays the setting of the Southern Marginal Zone, LGC is the Limpopo granulite complex, NMZ is the Northern Marginal Zone, CZ is the central zone, SMZ is the Southern Marginal Zone, KC is the Kaapvaal craton, and ZC is the Zimbabwe craton.

gneisses often developing after these rocks. The Beit Bridge Complex is dominated by leucocratic quartz–feldspar gneisses, which consist of perthitic potassic feldspar, biotite, hornblende, and hypersthene. The metasediments are metapelite gneisses, marbles, calc–silicate rocks, quartzites, and magnetite quartzites. The migmatized metapelitic gneisses often contain alternating layers with different mineral compositions. The relatively magnesian metapelites typically contain the assemblage *Opx* + *Crd* + *Grt* + *Qtz*, and more ferrous varieties bear *Crd* + *Grt* + *Qtz* + *Sil*. These two assemblages commonly have reaction textures of isobaric and/or decompressional cooling. In places, depending on the *P–T* parameters, both assemblages can be found in a single thin section (Perchuk *et al.*, 1996).

The final evolutionary stage of the Limpopo granulite complex was controlled by the emplacement of the Great Dike (2.46 Ga) into the metabasites of the Northern Marginal Zone and the intrusion of subvolcanic dikes of subalkaline granites into the tonalite gneisses of the Southern Marginal Zone (2450 Ma). This means that the rocks of the marginal zones of the Limpopo Complex occurred near the surface at approximately 2.46 Ga. At the same time, the absence of zircons with ages of 2.65–2.7 Ga (Dorland *et al.*, 2004) from the sedimentary rocks of Transvaal (de Wit *et al.*, 1992) provides evidence that the rocks of the Limpopo Complex were then not exposed at the surface.

D2/M2 metamorphism in the Limpopo Complex occurred in all of its zones, but we will consider below

only the Southern Marginal and Central zones. As was mentioned above, they include shear zones of ductile deformations (Fig. 4), which were produced simultaneously with the exhumation of the complex and were affected by extensive mylonitization and hydrothermal alterations (Smit and van Reenen, 1997; Smit *et al.*, 2001). The isotopic age of these alterations remains uncertain, but the morphology of the zones and the composition and textures of their rocks suggest that the zones were produced simultaneously with brittle deformations. The mylonites sometimes contain relict blocks of *straight gneisses*, which can be utilized to evaluate the *P–T* parameters during exhumation to middle and, in places, upper crustal levels. One of them is the Petronella zone, whose structural and petrotextural characteristics can be found in (Smit *et al.*, 2001). That paper presents the comparison of rocks from this zone with almost undeformed metapelite gneisses (Fig. 1c). The mineralogy of the deformed and undeformed gneisses is briefly considered below, along with the thermodynamic conditions of their crystallization and evolution, as is illustrated by the example of rock samples from the Petronella zone. We will also compare and analyze their *P–T* paths.

Southern Marginal Zone. Sample DR45 (see Fig. 4 for the sampling site location) is almost unaltered and consists of *Grt*, *Crd*, *Opx*, *Bt*, *Qtz*, *Pl*, and *Kfs* with minor amounts of accessory minerals (monazite, sphene, and zircon). No conspicuous traces of deformations were identified under the microscope, but *Qtz* and *Pl* inclusions in *Grt* porphyroblasts are oriented systematically (Fig. 5a) and similarly in all *Grt* grains. The core of this garnet was produced during the metamorphic culmination, because, in contrast to the outer zones, it contains oriented inclusions and is chemically homogeneous ($X_{Mg} \approx 0.51$, $X_{Ca} \approx 0.05$; Fig. 5c, inset), as also follows from its pale gray color in a BSE image (Fig. 5a). During exhumation the composition of the *Grt* grain systematically changed: the color of the mineral in the BSE image becomes progressively paler toward the rim (Figs. 5a, 5c, inset). Near contacts with matrix quartz, garnet porphyroblasts are surrounded by *Crd-Opx*$_2$ symplectitic rims, which in places have a very thin *Opx*$_2$ outermost shell (Fig. 5a). Symplectites occasionally penetrate into the intermediate portions of garnet grains along cracks (Fig. 5b). Figure 5c displays the *P–T* trajectory of the decompressional cooling deduced for metapelite DR45 based on the data of Table 1, which reports the compositions of minerals in local equilibrium (Perchuk *et al.*, 1996; Smit *et al.*, 2001). This trajectory is also plotted in the diagram of equal modal garnet concentrations (Fig. 5d). The intersections of isopleths of arbitrary garnet modes suggests a systematic decrease in the garnet concentration during the exhumation of the rock (Gerya, 1991) due to the shift of reaction (5) to the right-hand side, i.e., *Grt* + *Qtz* = *Opx*$_2$ + *Crd*.

In contrast to metapelite DR45, relics of *straight gneisses* (PET1, CAPR7, and CA1) from the Petronella ductile shear zone (Fig. 4) show all textural features of straight gneisses generated under induced motions rather than free ascent (Perchuk and Gerya, 2004). These gneisses look like the rocks displayed in Fig. 1d. These are linearly oriented rocks, often with flattened garnet (Fig. 6) rich in *Sil* and *Crd*$_1$ inclusions. The orientation of the sillimanite is always parallel to the schistosity of the gneiss and does not vary from grain to grain (Fig. 6a). The inclusions have likely been captured very early in the course of rock evolution, perhaps, even before the ductile deformations, i.e., during the (D2/D1)/(M2/M1) deformations. However, already this stage was characterized by the replacement of the assemblage *Grt*$_1$ + *Qtz* + *Sil* by the newly formed cordierite *Crd*$_2$ (Fig. 6a). In more magnesian metapelites, *Grt*$_1$ was replaced by *Opx* + *Crd*$_2$ symplectites with the almost complete decomposition of the garnet (Fig. 6b) during decompressional cooling (Harley, 1998; Perchuk, 1989; Perchuk *et al.*, 1996). The pseudomorphs inherit the lens-shaped flattened morphology from the garnet schistosity (Fig. 6b).

The newly formed *Grt*$_2$ + *Qtz* + *Sil* assemblage is produced via *Crd*$_2$ decomposition (Fig. 6c) during the subisobaric cooling of the rock (see, for example, Perchuk *et al.*, 1996). The subhedral young garnet (*Grt*$_2$) and undeformed *Qtz-Sil* symplectites testify to a long-lasting stage of subisobaric cooling (Fig. 6d) after the main deformation stage D2/M2. The maximum *P–T* parameters of cooling (Fig. 6d) are determined by the origin of *Grt*$_1$ lenses with relics of *Sil* and *Crd*, and the minimum parameters are marked by the development of euhedral *Grt*$_2$ and undeformed *Opx*$_2$ + *Crd*$_2$ symplectites (Figs. 6b, 6c). This suggests that the texture of the straight gneiss was produced within a relatively narrow range of *P–T* parameters, i.e., that the exhumation of the Limpopo Complex began in the Late Archean (~2.67 Ga). The *P–T* path of the straight gneisses from the Petronella zone (Fig. 6d) displays a fully pronounced segment of isobaric cooling that was not associated with any significant deformations.

The reader can find a fairly thorough characterization of the metamorphic events that produced the Limpopo straight gneisses and their evolution in (Smit *et al.*, 2001), but that paper does not characterize all relations between the *P–T* paths of these rocks and normal gneisses, an issue important for the accurate interpretation of the dynamic events. The key point here is the dating of ductile shear zones in the Southern Marginal Zone. Figure 4 demonstrates that the Matok granite pluton (~2.69 Ga) cuts across the N'Tabalala shear zone, which is dominated by typical mylonites

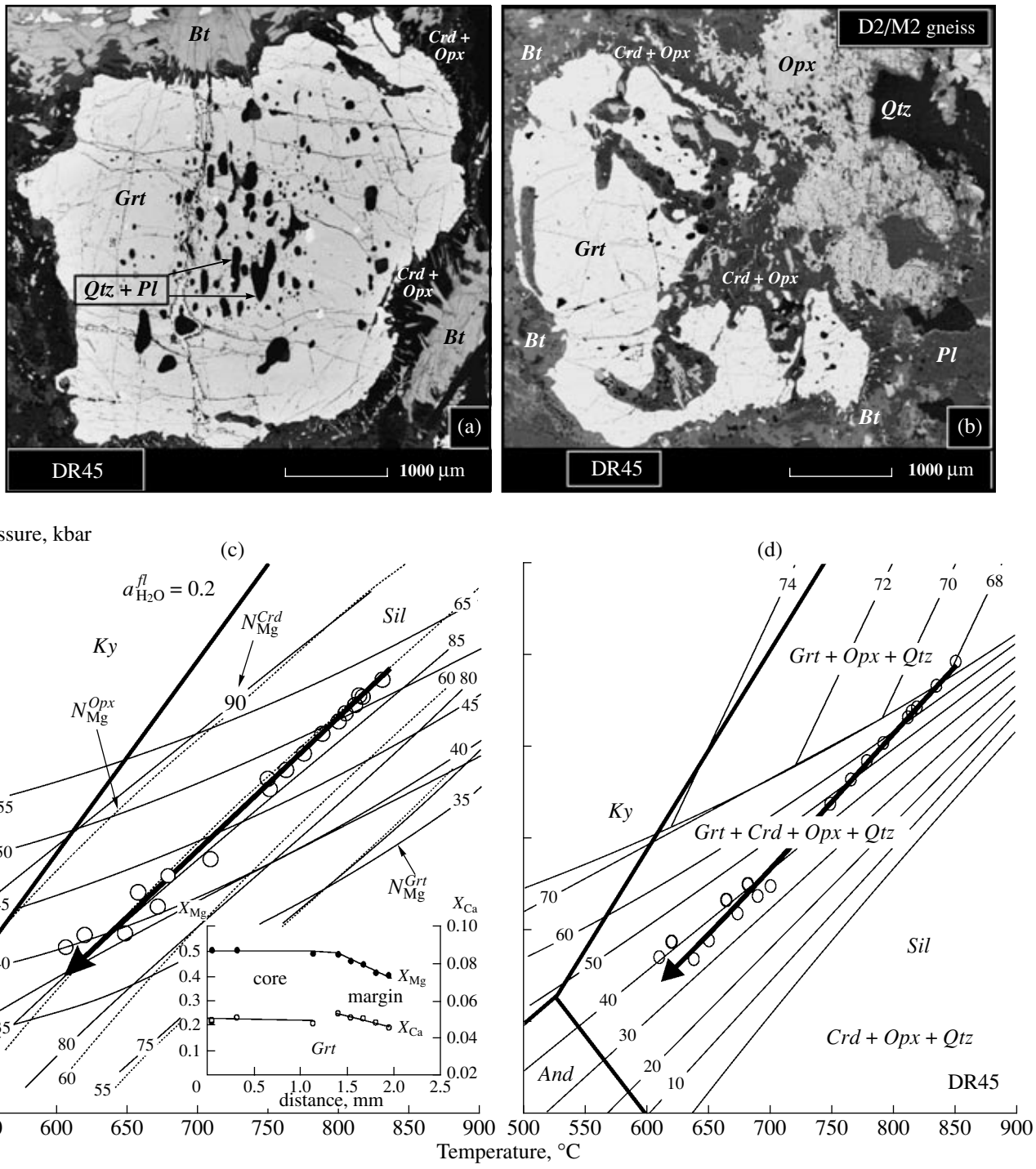

Fig. 5. Microtexture of gneiss DR45 (BSE image) from the Southern Marginal Zone of the Limpopo granulite complex and the *P–T* trajectories of its exhumation (after Perchuk *et al.*, 1996; Smit *et al.*, 2001). (a) Systematically oriented quartz inclusions in garnet that indicate the culmination metamorphic stage D2/M2; (b) reaction texture $Grt + Qtz \Rightarrow Opx_2 + Crd$ that developed during the exhumation of the Limpopo Complex (D2/M2) in the Late Archean (~2.67 Ga) in the absence of deformations; (c) *P–T* trajectory recorded in the mineral assemblage of gneiss DR45 and calculated based on the data of Table 1; (d) same *P–T* trajectory illustrating the systematic decomposition of *Grt* according to the reaction $Grt + Qtz \Rightarrow Opx_2 + Crd$ at decreasing *P–T* parameters (Gerya, 1991).

Figure 5a clearly demonstrates that the core and intermediate zones of the garnet grains with abundant mineral inclusions are light gray and become notably brighter toward crystal margins, and the relatively thin outermost zone (which is devoid of inclusions) is virtually white. This color distribution completely corresponds to the constancy of the garnet composition in the core and the gradual change in this composition in outer zones (inset in Fig. 5c) that overgrew the primary garnet of the composition $Grt_{0.51}$ during exhumation.

(Smit *et al.*, 2001). This implies that the pluton was emplaced after the transition from ductile to brittle deformations. However, the straight gneisses bear practically no high-temperature (>800°C) mineral assemblages but only pseudomorphs after them (see, for example, Fig. 6b). The synchronous exhumation of the straight gneisses with normal gneisses follows from the conjugated character of their *P–T* paths and similar isotopic ages (>2.69 Ga). Figure 7 displays the *P–T* trajectories of two samples: DR45 (Table 1, Fig. 5d) and PET1 (Table 2). The maxima of the *P–T* parameters coincide with the middle parts of the *P–T* trajectory for straight gneiss DR45, which shows no traces of ductile deformations. The exhumations of both rocks was, however, simultaneous, and, hence, the straight gneisses were formed in ductile shear zones separating vast blocks of undeformed granulites during their exhumation and cooling. Obviously, the cooling of rocks in these zones proceeded more rapidly than in the blocks, because the kinetic energy in the former was spent on heating in the course of intense ductile deformation. Analogous situations can be observed in all ductile shear zones that developed during various evolutionary stages of granulite complexes.

The *Central Zone* of the Limpopo Complex is polymetamorphic, and, hence, it is very difficult not only to identify its D2/M2 ductile shear zones consisting of straight gneisses but also to find fresh metapelite samples suitable for the derivation of their *P–T* trajectories. Nevertheless, a few such samples were found in the Beit Bridge Formation, whose Archean age was repeatedly confirmed by various isotopic techniques (see, for example, Hofmann *et al.*, 1998; Kröner *et al.*, 1998, 1999; Boshoff *et al.*, 2004). One of these samples (JP1) was thoroughly examined on a microprobe (Table 3). This sample was taken from the so-called cross fold of Baklykraal (van Reenen *et al.*, 2004). The rock is very fresh medium-grained massive gneiss with a massive structure and a granoblastic texture and consisting of the *Grt* + *Crd* + *Opx* + *Qtz* + *Bt* + *Pl* + *Zrn* mineral assemblage, practically without leucosome. The predominant porphyroblasts are garnet, cordierite, and orthopyroxene with quartz inclusions. Cleavage planes in orthopyroxene are often lined with tiny (a few micrometers long) sillimanite needles, which exsolved from the orthopyroxene during rock cooling. One garnet grain was determined to contain a cordierite inclusion, which provides evidence that the rock was metamorphosed (M2) within the cordierite stability field at $T = 900$°C (Table 4), which was favorable for a high Al_2O_3 solubility in orthopyroxene. The cordierite contains biotite inclusions (Bt_1). This mineral was also found as grains 0.4×0.9 mm in size (Bt_2). Garnet porphyroblast are surrounded by clearly developed reaction textures *Grt* + *Qtz* ⇒ *Crd* + *Opx* (Fig. 8, inset), which mark the final stage in the decompressional cooling of the rock. The composition and texture of the rock suggest its restitic nature.

Table 1. Compositions of the cores and marginal parts of mineral grains in the *Grt* + *Qtz* + *Opx* + *Crd* assemblage and the *P–T* parameters of their equilibria in undeformed metapelite DR45 from the Southern Marginal Zone of the Limpopo Complex (see Figs. 1 and 5)

Grt			*Opx*		*Crd*	*T*, °C	*P*, kbar
X_{Mg}	X_{Ca}	X_{Mn}	X_{Mg}	X_{Al}	X_{Mg}		
cores							
0.523	0.063	0.003	0.683	0.075		832	8.5*
0.514	0.060	0.006	0.683	0.075		817	8.5*
0.513	0.057	0.008	0.683	0.075		816	8.5*
0.511	0.054	0.006	0.683	0.075		812	8.5*
0.510	0.052	0.009	0.683	0.075	0.841	811	7.4
0.508	0.050	0.006	0.683	0.075	0.841	808	7.35
0.508	0.049	0.008	0.683	0.075	0.841	808	7.35
0.497	0.049	0.006	0.683	0.075	0.841	790	7.1
0.496	0.048	0.004	0.683	0.075	0.841	789	7.08
0.488	0.048	0.006	0.683	0.075	0.841	777	6.89
0.479	0.041	0.005	0.683	0.075	0.841	763	6.69
0.475	0.024	0.006	0.679	0.069	0.843	752	6.59
0.471	0.029	0.004	0.674	0.064	0.841	752	6.53
0.467	0.026	0.005	0.683	0.075	0.841	746	6.42
margins							
0.438	0.027	0.006	0.685	0.043	0.844	698	5.53
0.433	0.032	0.008	0.676	0.047	0.850	679	5.55
0.424	0.028	0.010	0.672	0.046	0.841	687	5.41
0.422	0.033	0.010	0.672	0.046	0.852	661	5.36
0.418	0.026	0.012	0.678	0.046	0.845	671	5.22
0.404	0.033	0.010	0.678	0.046	0.848	647	4.93
0.404	0.033	0.010	0.678	0.046	0.862	618	4.93
0.394	0.034	0.013	0.678	0.046	0.862	607	4.73
0.394	0.028	0.008	0.678	0.046	0.848	635	4.72

* Pressure values (Perchuk *et al.*, 1996) for which the temperatures were calculated by the experimentally calibrated *Opx–Grt* thermometer (Perchuk and Lavrent'eva, 1990).

The garnet is zonal: N_{Mg} in the cores reaches 60 mol % at a clearly pronounced flat zoning profile,

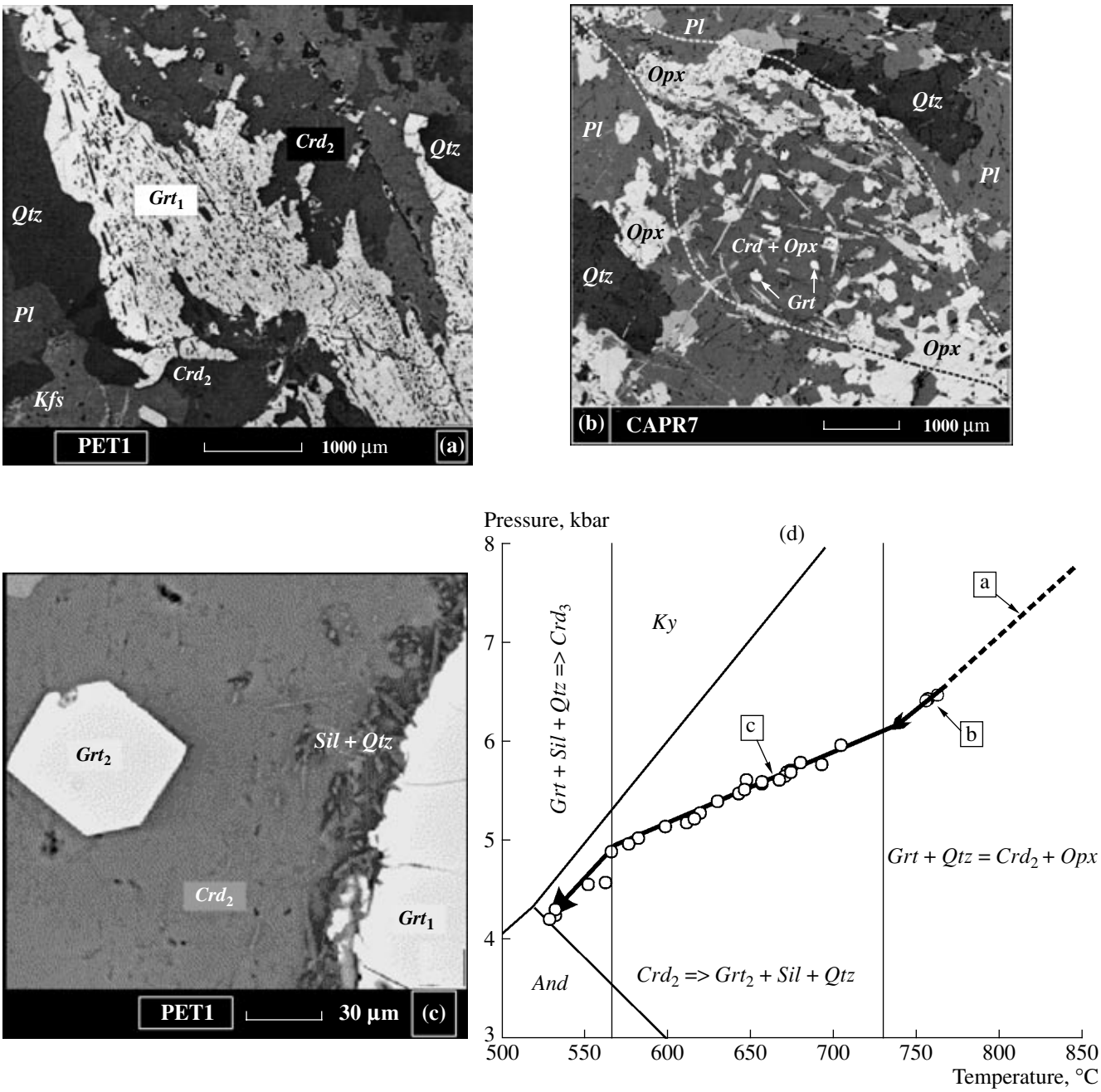

Fig. 6. Microtextures of straight gneisses (BSE images) from the Petronella ductile shear zone and the integral *P–T* trajectory of their exhumation during D2/M2 metamorphism (microtextures are compiled from Smit *et al.*, 2001). (a) *Sil* inclusions in garnet; inclusions are oriented parallel to the schistosity of the gneiss, and the orientation remains the same in all garnet grains. Sillimanite was most probably captured very early in the course of rock origin (M2/M1), perhaps, during the onset of ductile deformations (D2/D1). The images illustrate the initial replacement of the $Grt_1 + Qtz + Sil$ assemblage by *Crd*. (b) Relics of garnet in *Opx* + *Crd* symplectite from more magnesian straight gneiss CAPR7. (c) Development of a $Crd \Rightarrow Grt + Qtz + Sil$ reaction texture with newly formed euhedral garnet (Grt_2). The newly formed $Grt_2 + Qtz + Sil$ assemblage is produced by the decomposition of *Crd*, usually during subisobaric cooling. (d) Generalized *P–T* trajectory derived for a set of samples from the Petronella zone (Fig. 4). The isobaric segment of this trajectory is best consistent with the *P–T* trajectory for sample PET1 (Table 2). Arrows indicate the correspondence between the microtexture and the *P–T* parameters during various stages of the decompression and cooling of rocks from the Petropnella ductile shear zone.

and the pyrope concentration decreases to 48 mol % toward the margins. At contacts with symplectitic cordierite, N_{Mg}^{Grt} = 47 mol % (Table 3). The zoning of orthopyroxene and cordierite porphyroblast is much less clear and is pronounced in the outermost rims: N_{Mg}^{Opx} = 73 mol % in the cores of porphyroblasts and up

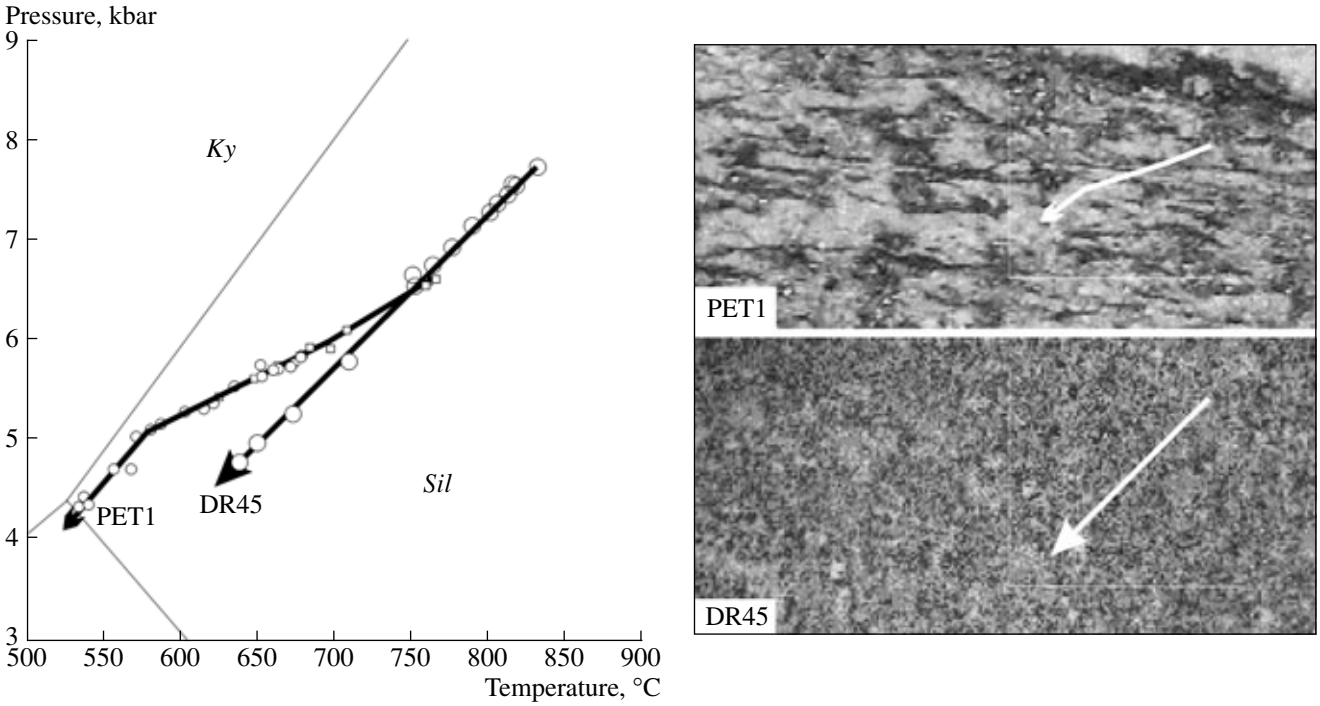

Fig. 7. *P–T* trajectories for normal undeformed gneiss D2/M2 (sample DR45, see Table 1 and Fig. 5d) and straight gneiss D2/M2 (sample PET1, Table 2).

The maximum *P–T* parameters of the exhumation of straight gneiss D2 occur in the middle segment of the *P–T* trajectory, which was recorded by local equilibria in sample DR45 (which displays no traces of ductile deformations: see photos to the right for the textures of this rock). The intersection of the *P–T* trajectories suggests that the rocks were exhumed simultaneously.

Table 2. Compositions of the cores and marginal parts of mineral grains in the *Grt* + *Qtz* + *Sil* + *Crd* assemblage and the *P–T* parameters of their equilibria in straight gneiss PET1 from the Southern Marginal Zone of the Limpopo Complex*

Grt			*Crd*	*T*, °C	*P*, kbar	*Grt*			*Crd*	*T*, °C	*P*, kbar
X_{Mg}	X_{Ca}	X_{Mn}	X_{Mg}			X_{Mg}	X_{Ca}	X_{Mn}	X_{Mg}		
cores						margins					
0.383	0.020	0.020	0.784	756	6.42	0.385	0.018	0.020	0.863	598	5.14
0.382	0.021	0.019	0.784	755	6.40	0.386	0.021	0.017	0.871	582	5.02
0.380	0.022	0.011	0.779	762	6.46	0.332	0.019	0.017	0.868	533	4.24
0.382	0.021	0.015	0.833	656	5.57	0.378	0.019	0.020	0.853	611	5.18
0.388	0.017	0.017	0.825	680	5.79	0.386	0.021	0.017	0.848	630	5.40
0.380	0.022	0.011	0.824	672	5.68	0.386	0.022	0.015	0.874	576	4.97
0.383	0.022	0.020	0.833	657	5.59	0.342	0.024	0.019	0.874	532	4.31
0.383	0.022	0.020	0.840	643	5.48	0.385	0.020	0.019	0.878	566	4.89
0.382	0.020	0.020	0.809	704	5.96	0.397	0.019	0.019	0.846	647	5.61
0.374	0.021	0.021	0.809	693	5.77	0.384	0.020	0.017	0.839	646	5.51
0.375	0.022	0.023	0.823	667	5.61	0.355	0.021	0.018	0.870	552	4.56
0.380	0.020	0.019	0.823	674	5.70	0.384	0.024	0.018	0.839	646	5.51
0.376	0.022	0.020	0.822	670	5.64	0.348	0.024	0.022	0.861	563	4.58
0.379	0.018	0.016	0.822	674	5.69	0.330	0.019	0.023	0.869	529	4.20
0.383	0.020	0.020	0.833	657	5.59	0.379	0.018	0.016	0.851	616	5.23
0.382	0.021	0.019	0.851	619	5.28						
0.376	0.022	0.020	0.824	667	5.61						

* See (Gerya, 1999; Smit *et al.*, 2001) for microprobe spot analyses of minerals.

Table 3. Selected microprobe analyses of minerals from sample JP1, Central Zone of the Limpopo Complex

Component	*Grt*	*Grt*	*Grt*	*Grt*	*Grt*	*Grt*	*Grt*	*Grt*	*Grt*	*Grt*	*Grt*	*Grt*	*Grt*	*Grt*
	P13	P16	P17	P18	P27	P28	P37	P41	P46	P52	P59	P60	P64	P29
SiO_2	39.46	40.16	39.76	39.93	40.22	40.23	39.49	39.44	39.59	40.13	39.78	39.88	39.71	40.25
TiO_2	0.00	0.04	0.00	0.00	0.00	0.15	0.02	0.04	0.00	0.09	0.00	0.00	0.00	0.00
Al_2O_3	22.18	22.44	22.47	22.16	22.19	22.28	21.85	21.84	22.01	22.24	22.39	22.18	22.40	22.49
FeO	23.72	20.94	21.53	21.29	20.99	21.58	24.20	24.37	23.26	22.01	22.43	22.26	22.32	23.45
MnO	0.36	0.37	0.20	0.38	0.30	0.06	0.38	0.42	0.37	0.15	0.35	0.48	0.19	0.58
MgO	12.02	14.31	14.40	14.28	14.46	13.90	12.30	12.12	13.14	13.67	13.28	13.47	13.67	12.42
CaO	2.07	1.70	1.56	1.69	1.82	1.73	1.49	1.63	1.47	1.60	1.73	1.63	1.52	1.54
Na_2O	0.19	0.05	0.07	0.20	0.02	0.05	0.27	0.15	0.16	0.09	0.00	0.10	0.18	0.17
K_2O	0.01	0.00	0.00	0.05	0.00	0.03	0.00	0.00	0.00	0.00	0.03	0.00	0.01	0.06
Proportions of cations														
Si	2.99	2.99	2.97	2.99	3.00	3.00	2.99	2.99	2.99	3.00	2.99	2.99	2.98	3.01
Ti	0.00	0.00	0.00	0.00	0.00	0.01	0.00	0.00	0.00	0.01	0.00	0.00	0.00	0.00
Al	1.98	1.97	1.98	1.95	1.95	1.96	1.95	1.95	1.96	1.96	1.98	1.96	1.98	1.98
Fe^{2+}	1.50	1.30	1.34	1.33	1.31	1.35	1.53	1.55	1.47	1.38	1.41	1.40	1.40	1.46
Mn	0.02	0.02	0.01	0.02	0.02	0.00	0.02	0.03	0.02	0.01	0.02	0.03	0.01	0.04
Mg	1.36	1.59	1.60	1.59	1.61	1.54	1.39	1.37	1.48	1.52	1.48	1.51	1.53	1.38
Ca	0.17	0.14	0.13	0.14	0.15	0.14	0.12	0.13	0.12	0.13	0.14	0.13	0.12	0.12
Na	0.03	0.01	0.01	0.03	0.00	0.01	0.04	0.02	0.02	0.01	0.00	0.02	0.03	0.02
K	0.00	0.00	0.00	0.01	0.00	0.00	0.00	0.00	0.00	0.00	0.00	0.00	0.00	0.01
X_{Mg}	0.47	0.55	0.54	0.54	0.55	0.53	0.48	0.47	0.50	0.53	0.51	0.52	0.52	0.49
X_{Ca}	0.06	0.04	0.04	0.04	0.05	0.05	0.04	0.04	0.04	0.04	0.05	0.04	0.04	0.08
X_{Al}														
Component	*Opx*	*Opx*	*Opx*	*Opx*	*Opx*	*Opx*	*Opx*	*Opx*	*Crd*	*Crd*	*Crd*	*Crd*	*Crd*	*Crd*
	P11	P15	P31	P33	P40	P42	P43	P47	P30	P32	P39	P44	P63	P65
SiO_2	51.60	51.67	52.14	51.68	53.30	52.53	51.35	51.89	49.62	49.69	49.45	49.99	49.43	49.24
TiO_2	0.12	0.35	0.22	0.17	0.08	0.13	0.07	0.10	0.00	0.00	0.00	0.10	0.02	0.00
Al_2O_3	5.79	5.36	5.62	4.94	2.21	3.72	5.57	5.36	33.09	32.86	32.65	32.93	32.72	32.33
FeO	17.20	17.10	16.99	18.37	19.21	19.53	17.84	18.88	2.83	3.02	3.00	3.09	3.33	3.12
MnO	0.14	0.02	0.11	0.24	0.07	0.10	0.17	0.17	0.05	0.13	0.00	0.09	0.00	0.05
MgO	25.75	25.92	25.90	24.51	25.58	25.00	25.01	25.25	11.43	10.93	11.09	11.60	11.05	10.79
CaO	0.10	0.11	0.11	0.10	0.16	0.14	0.12	0.11	0.05	0.03	0.03	0.03	0.01	0.05
Na_2O	0.31	0.13	0.17	0.06	0.21	0.26	0.15	0.16	0.11	0.08	0.06	0.18	0.11	0.08
K_2O	0.04	0.00	0.00	0.02	0.00	0.00	0.00	0.01	0.03	0.00	0.00	0.00	0.00	0.00
Total	101.05	100.67	101.24	100.09	100.83	101.41	100.28	101.91	97.21	96.73	96.29	98.00	96.68	95.65
Proportions of cations														
Si	1.85	1.86	1.87	1.88	1.94	1.90	1.86	1.86	5.04	5.07	5.06	5.04	5.05	5.08
Ti	0.00	0.01	0.01	0.00	0.00	0.00	0.00	0.00	0.00	0.00	0.00	0.01	0.00	0.00
Al	0.25	0.23	0.24	0.21	0.09	0.16	0.24	0.23	3.96	3.95	3.94	3.91	3.94	3.93
Fe^{2+}	0.52	0.52	0.51	0.56	0.58	0.59	0.54	0.57	0.24	0.26	0.26	0.26	0.28	0.27
Mn	0.00	0.00	0.00	0.01	0.00	0.00	0.01	0.01	0.00	0.01	0.00	0.01	0.00	0.00
Mg	1.38	1.39	1.38	1.33	1.38	1.35	1.35	1.35	1.73	1.66	1.69	1.74	1.68	1.66
Ca	0.00	0.00	0.00	0.00	0.01	0.01	0.00	0.00	0.01	0.00	0.00	0.00	0.00	0.01
Na	0.02	0.01	0.01	0.00	0.01	0.02	0.01	0.01	0.02	0.02	0.01	0.04	0.02	0.02
K	0.00	0.00	0.00	0.00	0.00	0.00	0.00	0.00	0.00	0.00	0.00	0.00	0.00	0.00
X_{Mg}	0.73	0.73	0.73	0.70	0.70	0.70	0.71	0.70	0.88	0.87	0.87	0.87	0.86	0.86
X_{Ca}	0.00	0.00	0.00	0.00	0.00	0.00	0.00	0.00	0.00	0.00	0.00	0.00	0.00	0.00
X_{Al}	0.053	0.023	0.039	0.059	0.056	0.039	0.059	0.056	0.88	0.87	0.87	0.87	0.86	0.86

Table 4. Mole fractions of some components in minerals from sample JP1 and the *P–T* parameters of their equilibria calculated at $a^{fl}_{H_2O} = 0.2$ (Central Zone of the Limpopo Complex)

Grt			*Opx*			*Crd*		*T*, °C	*P*, kbar
analytical spot	X_{Mg}	X_{Ca}	analytical spot	X_{Mg}	X_{Al}	analytical spot	X_{Mg}		
cores									
R38	0.595	0.035	P33	0.704	0.053	P63	0.855	914	9.0
R37	0.577	0.039	P33	0.704	0.053	P63	0.855	880	8.5
R36	0.564	0.037	P33	0.704	0.053	P63	0.855	856	8.2
P16	0.549	0.045	P33	0.704	0.053	P63	0.855	831	7.8
P27	0.551	0.048	P33	0.704	0.053	P65	0.861	816	7.8
P18	0.545	0.044	P33	0.704	0.053	P63	0.855	824	7.7
P17	0.544	0.041	P33	0.704	0.053	P65	0.861	804	7.6
P28	0.534	0.046	P33	0.704	0.053	P32	0.866	774	7.4
P52	0.525	0.042	P33	0.704	0.053	P32	0.866	761	7.2
P64	0.522	0.040	P33	0.704	0.053	P65	0.861	771	7.2
P60	0.519	0.043	P33	0.704	0.053	P63	0.855	783	7.1
P59	0.513	0.046	P33	0.704	0.053	P63	0.855	774	7.0
P46	0.502	0.039	P33	0.704	0.053	P32	0.866	728	6.7
P45	0.497	0.039	P33	0.704	0.053	P32	0.866	722	6.6
margins									
P37	0.475	0.040	P42	0.695	0.039	P39	0.868	687	6.1
P29	0.486	0.041	P31	0.731	0.059	P30	0.878	675	6.1
P37	0.475	0.040	P43	0.714	0.059	P39	0.868	687	6.1
P41	0.470	0.043	P47	0.704	0.056	P44	0.870	677	6.0
P13	0.475	0.055	P11	0.727	0.061	P12	0.874	672	5.9
P13	0.475	0.055	P15	0.730	0.056	P12	0.874	672	5.9
P41	0.470	0.043	P40	0.704	0.023	P44	0.870	676	5.9

to 75 mol % in their margins, and $N^{Crd}_{Mg} = 86$ mol % in cores and 88.5 mol % in margins. The N^{Crd}_{Mg} of garnet in contact with symplectitic cordierite reaches 91 mol %, which testifies to diffusion-controlled exchange between this mineral and garnet. The Al_2O_3 concentration in the *Opx* is no higher than 6 wt %. The biotite Bt_2 is also largely zonal, with the character of its zoning controlled by minerals occurring in contact with biotite. For example, a Bt_2 grain between *Crd* and *Opx* has an asymmetric zoning: $X^{Bt_2}_{Mg} = 0.731$ (at 1.44 f.u. of Al) in contact with orthopyroxene and $X^{Bt_2}_{Mg} = 0.8$ (at 1.59 f.u. of Al) in contact with cordierite. The number of Al atoms is directly correlated with $X^{Bt_2}_{Mg}$: Al (f.u.) = $2.0547 X^{Bt_2}_{Mg} - 0.077$, which is very unusual for metamorphic biotite (compare with data in Aranovich, 1991).

Table 4 reports the compositional and thermodynamic parameters of minerals from sample JP1. As can be seen, the maximum (peak) metamorphic temperature at $a^{fl}_{H_2O} = 0.2$ was close to 900°C, and the pressure was approximately 9 kbar. The minimum temperature of rock cooling was ~670°C at a pressure of ~5.9 kbar. The data of Table 4 were used to calculate a *P–T* trajectory for decompressional cooling (Fig. 8).

Dynamometamorphism D3/M3 in the Limpopo Complex is determined by the relations of the straight gneisses of the latest deformational event (D3/M3) with the straight and normal gneisses of deformational stage D2/M2. We have already mentioned above that Fig. 1 displays the textural differences between these gneisses. These differences are also discernible in the compositional parameters of coexisting Fe–Mg minerals from these rocks, which testify that the minerals have crystallized at different temperatures.

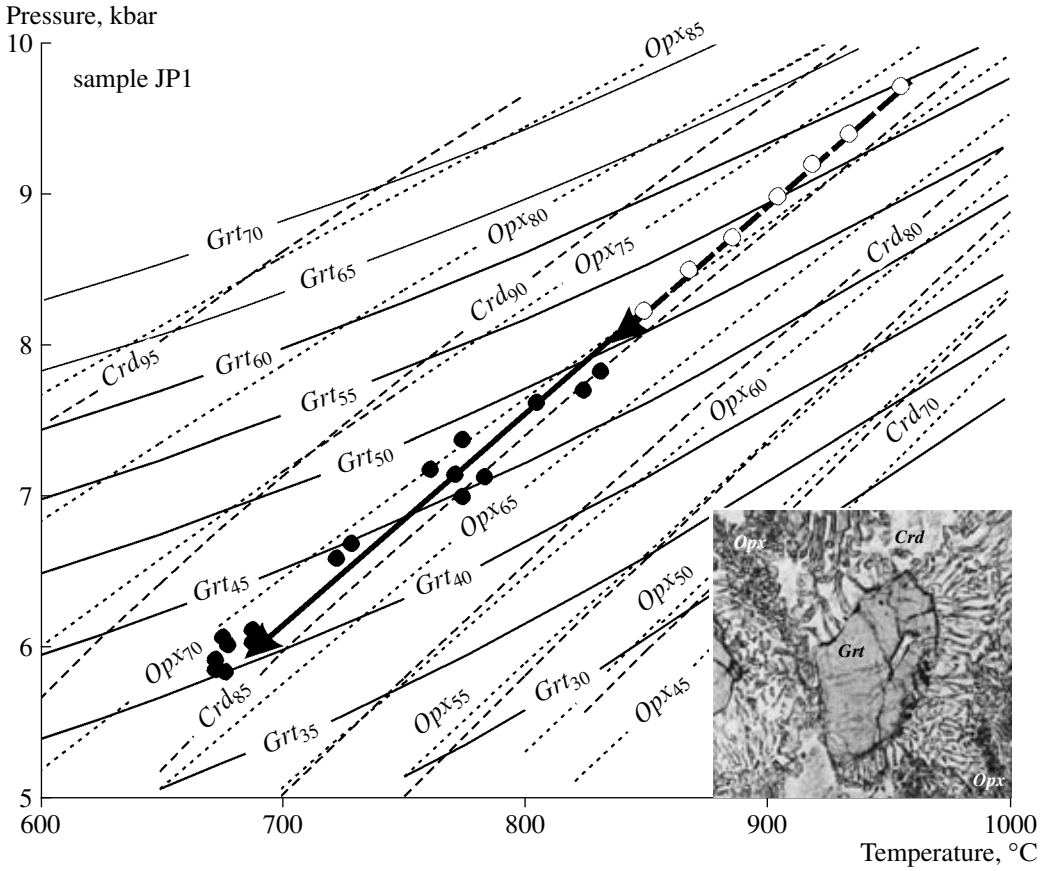

Fig. 8. *P–T* trajectory of the buoyant ascent of granulite from the lower continental crust to the middle crust [sample JP1, ~2.6 Ga, Central Zone of the Limpopo Complex (Baklykraal structure), South Africa; van Reenen *et al.*, 2004]. The inset displays a $Grt + Qtz \Rightarrow Crd_2 + Opx_2$ reaction texture (1.5 × 1.5 mm) in sample JP1. See Table 3 for analytical data and Table 4 for the calculated *P–T* parameters of local mineral equilibria according to reaction (1). The dashed-line part of the *P–T* trajectory (with open circles) traces the evolution of the *P–T* parameters during the buoyant ascent of the granulite, and the solid line (and solid circles) corresponds to the development of reaction texture (1). The high *P–T* parameters ($T > 850$°C, $P > 8.5$ kbar) were obtained for the cores of garnet, cordierite, and orthopyroxene porphyroblasts that were not involved in the production of symplectites. A mineralogical indication of the originally high temperature is the occurrence of sillimanite needles along cleavage plane in orthopyroxene. The garnet contains inclusions of early cordierite (Crd_1).

The detailed structural and geochronologic study of the granitoids and leucosome in the gneisses from the Central Zone (Hofmann *et al.*, 1998; Kröner *et al.*, 1998) has revealed that this zone is made up of polymetamorphic rocks. Their isotopic dates are notably different, a fact that still has not find any realistic geological interpretation. The youngest metamorphic event is dated at ~2 Ga (see, for example, Holzer *et al.*, 1998; Boshoff *et al.*, 2004) and has affected only the rocks of the Central Zone of the Limpopo granulite complex. It is thought (Kröner *et al.*, 1998, 1999) that stage D3/M3 was related not to an orogenic but to a "static" event. The mechanism of this "static" event is not discussed in the aforementioned publications. The results recently obtained in (Hisada *et al.*, 2005) indicate that the metamorphism of these rocks has been related to intense hydrothermal activity that locally affected these rocks. It was determined that this activity was spatially restricted to widespread D3 ductile shear zones, which were dated at approximately 2 Ga and are often overprinted onto D2 ductile shear zones. The fluid activity largely played a catalytic role in the mineral reactions, similarly to aqueous fluids in the processes of Phanerozoic eclogitization of Archean granulites (see, for example, Udovkina, 1972; Austrheim and Griffin, 1985).

The Central Zone of the Limpopo Complex contains roughly equal amounts of rock associations with ages of ~2.6 and ~2 Ga. Most of the older rocks (D2/M2) were variably affected by diaphthoresis. As was mentioned above, diaphthoresis overprinted both the D2/M2 and the D3/M3 rocks. Diaphthoresis manifests itself mostly in the form of mineral hydration: the replacement of orthopyroxene by cummingtonite, amphibole by chlorite, cordierite penitization, etc. However, relatively fresh straight gneisses are quite

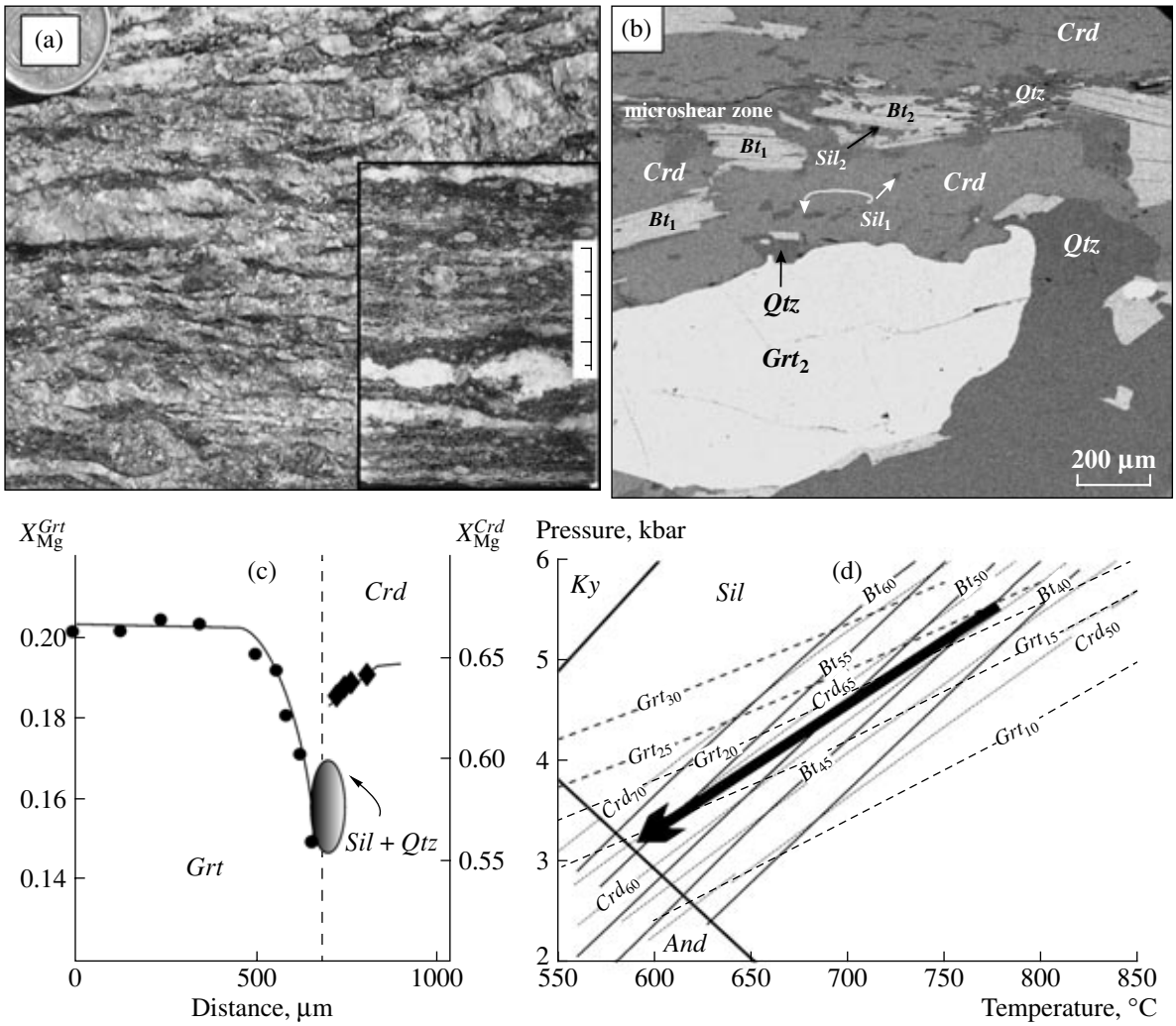

Fig. 9. Textural, chemical, and *P–T* characteristics of the exhumation conditions of a straight gneiss from a D3 dynamometamorphism zone (~2 Ga; Boshoff *et al.*, 2004) in the Central Zone of the Limpopo Complex (Baklykraal structure), South Africa (van Reenen *et al.*, 2004). (a) Microtexture of a straight gneiss demonstrating a linear orientation of all structural features; (b) microtexture of the same sample, consisting of *Crd* + *Grt* + *Sil* + *Qtz* + *Bt* + *Kfs*; it can be seen that the garnet grain contains no inclusions, is elongated conformably with the schistosity of the rock and is characterized by the development of replacing cordierite only on one side of the garnet grain; the thin fracture in the upper part of the photograph consists of *Sil* + *Qtz* + *Bt*; (c) chemical zoning of garnet and cordierite in contact with a replacement structure; it can be seen that the Mg mole fractions of both minerals decrease due to the shift of the reaction *Grt* + *Sil* + *Qtz* ⇒ *Crd* to the right with decreasing pressure; (d) *P–T* trajectory calculated based on the results of microprobe profiling of a number of garnet grains in contact with cordierite (diffusion zoning was ignored; van Renen *et al.*, 2004). Analytical data are presented in Table 5, and the compositions of locally equilibrated minerals are listed in Table 6.

common among the rocks of this complex. They occur in the form of shear zones in mafic and biotite–garnet gneisses and also as boudins in quartzites and marbles. These are always strongly sheared rocks with broken quartz–plagioclase leucosome and slightly elongated grains of pink garnet (Fig. 9a). In fresh rock samples, the usual mineral assemblage *Bt* + *Grt* + *Qtz* + *Crd* + *Sil* + *Kfs* + *Pl* ± *Ms* + *Rt* + *Zrn* is fairly stable, but most of the rocks are strongly hydrated, their cordierite is completely penitized, and biotite is sometimes replaced by chlorite. The two noteworthy textural features of these rocks are (1) the preferable replacement of garnet by cordierite only on one side of garnet grains, a feature that imparts elongated shapes to the garnet Grt_2 grains (Fig. 9b), and (2) the extensive development of the aforementioned tiny acid leaching zones along the schistosity, with these zones consisting of quartz, sillimanite, and biotite. The generation Grt_2 (~2027 Ma) strongly dominates in the rocks (Boshoff *et al.*, 2004), but relics of Grt_1 can also be found. The metapelite is an absolutely fresh, slightly more ferrous rock (van Reenen *et al.*, 2004), without any petrographic or textural traces of the earlier metamorphism that affected the surrounding rocks with an age of ~2.65 Ma (Boshoff *et al.*, 2004). The morphology of the crystals of Grt_2 is very diverse: they range from euhedral to pen-

cil- and atoll-shaped. Relict Grt_1 crystals are elongated conformably with the general schistosity of the rock and sometimes practically disappear, being nearly completely replaced by cordierite with $X_{Mg}^{Crd_2} = 0.74$ at contacts with relict garnet and $X_{Mg}^{Crd_2} = 0.7–0.69$ near the margins of the pseudomorphs. In places, they have unusual shapes, resembling a hat in cross section, which is possible only if the cordierite replaced atoll garnet: the inner portions of the atoll semicircles consist of quartz, sillimanite, and biotite; and their outer parts are in contact with matrix biotite and quartz. If the garnet occurred in a *Sil-Qtz* matrix early in the course of its replacement, cordierite was produced by the reaction $Grt + Sil + Qtz \Rightarrow Crd$ (6) evenly over the whole volume of the crystal, up to the nearly complete replacement of the garnet. This process produced complete cordierite pseudomorphs after garnet with quartz and biotite inclusions (van Reenen *et al.*, 2004, p. 1420, Fig. 4d). These aggregates are not deformed and not restricted to the schistosity, and thus, they were produced during isobaric heating and/or during the exhumation of the rock. However, most of the garnet grains are lens-shaped, elongated conformably with the rock schistosity, with reaction textures growing only on one side according to scheme (6) (Fig. 9b). We failed to identify the earliest cordierite (Crd_1); Crd_3 is more ferrous than Crd_2 and has reversed zoning: its $X_{Mg}^{Crd_3}$ decreases toward garnet from 0.7 to 0.67. Biotite occurs in all of our thin sections in two generations. The first of them (Bt_1) comprises large, up to 1 mm long, crystals in equilibrium with garnet and the matrix minerals of the rock ($Sil + Kfs + Pl + Qtz$). The second generation (Bt_2) comprises small flakes (a few dozen micrometers long) oriented along the rock schistosity (Fig. 9b). Bt_2 is restricted to very thin (micrometer-sized) shear zones (van Reenen *et al.*, 2004, Figs. 3a and 4f therein), in which it coexists with Sil_2 and Qtz. Potassic feldspar is rare and occurs in the rock matrix, together with $Sil + Bt_1 + Pl + Qtz$ and garnet porphyroblasts in this matrix. In one of our samples (T73), the rock matrix contains muscovite, which develops around feldspar and biotite near contacts with sillimanite. This implies its metamorphic genesis according to the classic reaction $Sil + Kfs + H_2O = Ms + Qtz$.

All of the Fe–Mg minerals are zoned. The concentration of the pyrope end member in the garnet decreases from grain cores to margins: N_{Mg}^{Grt} equals 21 mol % in the cores and ≥13.6 mol % in the margins. Garnet cores up to 1 mm in diameter typically display flat compositional profiles with $N_{Mg}^{Grt} = 21$ mol % (Fig. 9c). This is the highest value, which testifies that the garnet cores were formed at the peak of the regional metamorphism. The cordierite has an almost unchanging composition ($N_{Mg}^{Crd} = 61–64$) due to the opposite effects of temperature and pressure on its exchange equilibrium (1) with garnet and its discontinuous reaction (5). The composition of Bt_1 varies quite noticeably: 55.1 mol % > N_{Mg}^{Bt} > 44.6 mol %, whereas Bt_2 is more ferrous. Van Reenen *et al.* (2004) has demonstrated that the compositional variations in all of the minerals are strictly correlated with the variations in P, T, and $a_{H_2O}^{fl}$ (the latter parameter ranges from 0.26 to 0.31).

The compositional and thermodynamic parameters of local mineral equilibria from the metapelites T18, T20, and T73 are listed in Table 5. Figure 9d demonstrates the $P–T$ trajectory, which is based on these data, for the exhumation of rocks in the Baklykraal structure. The metamorphic culmination corresponded to $P \sim 5.8$ kbar and $T \sim 780$°C. Hence, the rocks were displaced within the Early Proterozoic crust from depths of about 18 km to approximately 10–11 km and simultaneously cooled by 190°C (the lowest temperature of the $P–T$ path). The wide occurrence of cordierite porphyroblasts with garnet relics suggests that the rock was significantly heated (from ~650–680 to 780°C) under a roughly constant pressure (of about 5.8 kbar). This is shown in Fig. 10a, in which the $P–T$ trajectories from Figs. 8 and 9d can be compared. It can be seen that, at $P = 5.8$ kbar, $T_{max} = 780$°C for the trajectory of the Early Proterozoic (~2 Ga) metapelites (Fig. 9d) corresponds to $T_{min} = 675$°C for the trajectory of the supposedly Late Archean (~2.6 Ga) granulites (Fig. 8). These $P–T$ paths are principally different from those in Fig. 7 for the straight and normal gneisses in the Southern Marginal Zone of the Limpopo Complex. While the geodynamic interpretation of the $P–T$ trajectories for the Southern Marginal Zone is quite simple (Perchuk and Gerya, 2004), an analogous interpretation for the coupled $P–T$ paths in Fig. 10 is not as obvious. Mineralogically similar metapelite samples from a single geological structure were taken from closely spaced sites. It is, however, pertinent to recall that no final conclusion about the folded nature of these structure was drawn as of yet. It was hypothesized (S. Smit, personal communication) that they are a system of Early Proterozoic *en-echelon* dynamometamorphic zones that cut across the sublatitudinal system of Archean folded structures, which are strongly dominated by sheath folds (Fig. 1a).

GEOCHRONOLOGIC PROBLEMS IN RELATION TO THE HIGH-TEMPERATURE POLYMETAMORPHISM OF PRECAMBRIAN GRANULITE COMPLEXES

The arguments presented above in support of the existence of Z-shaped $P–T$ trajectories for high-temper-

Table 5. Selected compositional and thermodynamic parameters of local equilibrium (2) for minerals from straight gneisses T18, T20, and T73 from the Baklykraal structure in the Central Zone of the Limpopo Complex (based on data from van Reenen *et al.*, 2004)

X_{Mg}^{Crd}	X_{Mg}^{Grt}	*T*, °C	$a_{H_2O}^{fl}$	*P*, kbar	X_{Mg}^{Crd}	X_{Mg}^{Grt}	*T*, °C	$a_{H_2O}^{fl}$	*P*, kbar
0.614	0.231	786	0.325	5.68	0.679	0.185	608	0.288	3.41
0.625	0.237	781	0.326	5.69	0.696	0.210	631	0.281	3.89
0.614	0.228	779	0.327	5.59	0.693	0.217	646	0.276	4.09
0.640	0.228	740	0.335	5.22	0.700	0.236	669	0.267	4.51
0.623	0.214	736	0.336	5.05	0.718	0.267	694	0.259	5.02
0.611	0.208	727	0.338	4.90	0.698	0.270	729	0.250	5.31
0.632	0.208	712	0.342	4.76	0.688	0.270	745	0.249	5.34
0.629	0.205	710	0.342	4.72	0.703	0.294	763	0.238	5.88
0.626	0.202	708	0.343	4.68	0.614	0.168	653	0.355	3.78
0.623	0.200	708	0.343	4.66	0.620	0.168	646	0.357	3.72
0.627	0.203	708	0.343	4.69	0.645	0.180	640	0.358	3.81
0.612	0.189	700	0.344	4.48	0.659	0.180	623	0.362	3.66
0.629	0.196	692	0.346	4.46	0.621	0.156	620	0.362	3.33
0.620	0.188	688	0.347	4.33	0.621	0.146	599	0.367	3.02
0.627	0.191	685	0.348	4.34	0.629	0.146	591	0.369	2.95
0.610	0.178	679	0.349	4.14	0.661	0.243	737	0.336	5.35
0.620	0.184	679	0.349	4.21	0.681	0.230	685	0.348	4.77
0.637	0.194	678	0.349	4.30	0.670	0.245	728	0.338	5.28
0.620	0.179	669	0.351	4.06	0.681	0.205	641	0.358	4.15
0.620	0.177	665	0.352	3.99	0.688	0.234	683	0.348	4.79

ature strike-slip deformations in viscous media should have left traces in many Precambrian metamorphic complexes. Such *P–T* paths are already known for some of them, and unusual geological relations have been established for their rocks with different isotopic dates. Other complexes show no significant traces of polymetamorphism, but Z-shaped *P–T* paths were derived for them, too. Some complexes are characterized by a diversity of *P–T* trajectories derived for them, but only one metamorphic cycle was dated in them (as in the Southern Marginal Zone of the Limpopo Complex). The reasons for this diversity were explained (see, for example, Perchuk *et al.*, 1996, 2001b). At the same time, there are granulite complex for which the rule "one complex—one *P–T* path" was proved valid. Below we consider examples that rather put forth tasks for geochronologic studies than settle geodynamic problems in the evolution of granulite complexes.

Sharyzhalgai Complex, southwestern Baikal area. The diverse rocks of these complex, their petrography and geochemistry were described in much detail in (Petrova and Levitskii, 1984). The cross section of the complex in the coastal exposures of Lake Baikal consists of a series of granite–gneiss domes, whose cores are composed of undeformed biotite granites and contain skialiths (remnants) of gneisses. The contact rocks are gneissose, up to the development of straight gneisses. The rocks between the domes are various members of the charnockite–enderbite series, biotite–garnet gneisses, metapelites, metabasalts, and carbonate rocks. These rocks are also often gneissose. Most gneisses of this complex have usual schistose structures and granoblastic textures, and some of the metapelites have characteristic reaction textures of type (7). The number of ductile shear zones is not great, but the rocks composing these zones display all features of straight gneisses. We have examined practically all rock varieties from the coastal exposures of Lake Baikal. The samples selected for the calculation of *P–T* trajectories represent normal and straight gneisses with the *Opx-Grt-Crd* and *Crd-Grt-Qtz-Sil* assemblages. These samples were described in detail in (Perchuk, 1989; Gerya, 1999). Sample BL3M3A is particularly interesting: its textural features resemble those of metapelite T73 from the Baklykraal structure of the Central Zone, Limpopo Complex (compare Figs. 11b and 9a), but the rock contains the assemblage *Opx* + *Grt* + *Crd* + *Qtz* + *Pl* + *Bt* + *Ilm* + *Zrn* and well developed reaction textures of type (5) (Perchuk, 1989). The rock has a typical blastomylonitic texture, with *Crd* and *Opx* reaction rims around garnet at its contacts with bluish quartz, easily

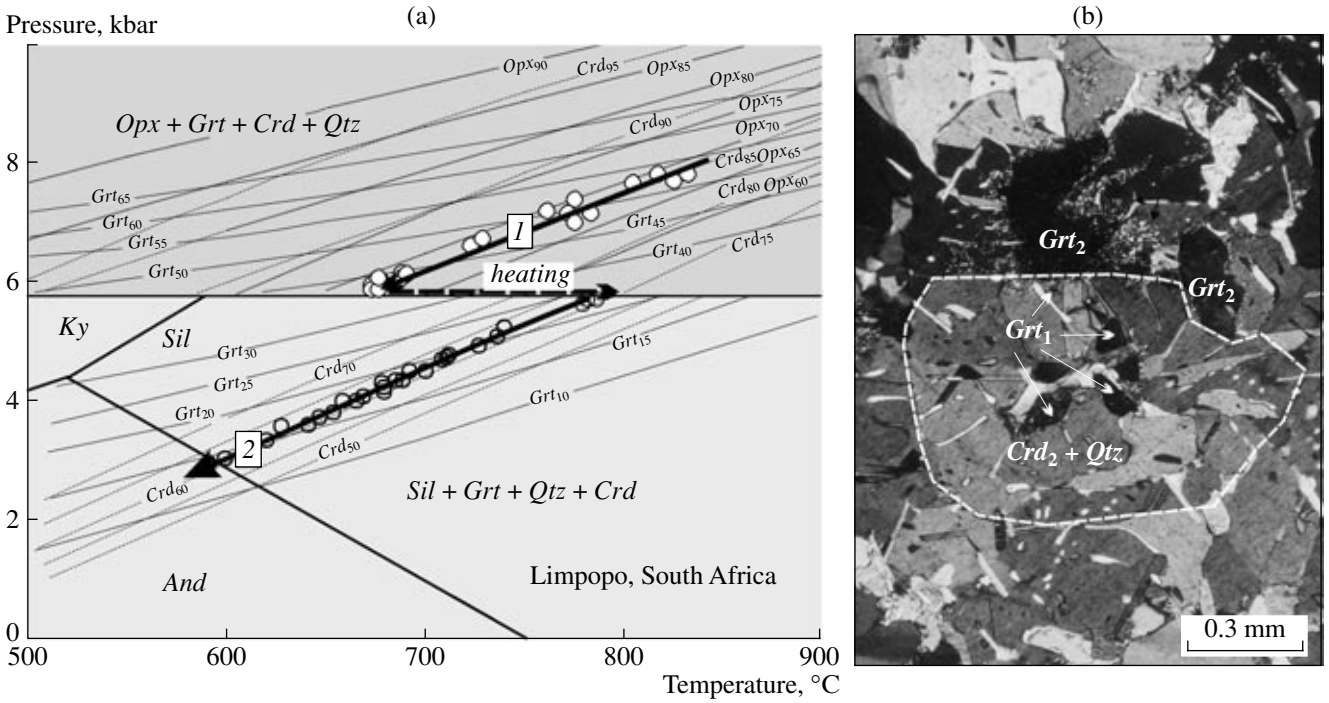

Fig. 10. Integral diagram of the *P–T* trajectories for the exhumation of normal (trajectory *1*, see Fig. 8) and straight (trajectory *2*, see Fig. 9d) metapelite gneisses in various geological times within the same Baklykraal geological structure (van Reenen *et al.*, 2004). The sampling sites of the gneisses are spaced ~100 m apart. Diagram in Fig. 10a demonstrates that the minimum temperature in the upper trajectory corresponds to a maximum temperature in the lower trajectory. This implies that the rocks were transformed (D3/M3) due to isobaric heating by ~120°C, supposedly ~600 m.y. after the first deformation–metamorphic (D2/M2) event. (b) Microphotograph (crossed polarizers) of a thin section of metapelite T20 displaying a nearly complete pseudomorph of cordierite (Crd_2) after primary garnet (Grt_1) according to reaction (6). See text for details.

discernible with the naked eye (Fig. 11b). Analogous relations can also be seen in thin sections, which display evidence of two stages of the textural evolution of this rock: the reaction texture $Qtz + Grt_1 \Rightarrow Opx + Crd_1(Pl_1)$ with relict *Kfs* + *Rt* + *Zrn* are surrounded by a fine-grained material of Grt_2, *Bt*, *Qtz*, Pl_2, Crd_2, and *Ilm*. The *Crd* in the symplectitic aggregates is rich in CO_2 and fresh, and the quartz contains abudant *Rt* needles. Both cordierite generations typically have wedge-shaped twins, pleochroic halos, and mosaic extinction. Double polished platelets prepared of this rock demonstrate that *Qtz*, *Pl*, and *Crd* contain inclusions of liquid CO_2. It was demonstrated (Perchuk, 1989) that a high $\mu^{fl}_{CO_2}$ had precluded the chloritization and sericitization of this cordierite, alterations that are widespread in other complexes. The mineral assemblage of the second generation is characterized by widespread Pl_2 and Crd_2 at contacts with *Qtz* and by the replacement of low-Ti Bt_1 by absolutely fresh Crd_2 without newly formed *Kfs*. Table 6 reports representative microprobe analyses of minerals from this straight gneiss, and Fig. 11 displays its microtexture (Fig. 11a), the chemical zoning of its garnet (Fig. 11c), and the *P–T* path (Fig. 11d), which was calculated based on the data of Table 7. This table generalizes the parameters of local equilibria in two samples from ductile shear zones in the Sharyzhalgai Complex. In contrast to the straight gneiss sample described above, metapelites B244 and B245, which are made up of the same mineral assemblage, have schistose structures and normal granoblastic textures. These rocks display well pronounced undeformed leucosome. Chemical analyses of minerals coexisting in these metapelites are listed in Table 8, and Table 9 presents the calculated *P–T* parameters of local equilibria. These data and information on some analogous samples (Gerya, 1999) were used to calculate the upper part of the *P–T* path in the diagram of Fig. 12.

The polymetamorphic nature of the Sharyzhalgai Complex is widely known, but its *P–T* trajectories shown in Fig. 12 were not dated, and, in spite of the published models (see, for example, Aftalion *et al.*, 1991), the geodynamic history of this complex cannot be considered known even in general terms. However, there are no other granulite complexes examined isotopically as thoroughly as the Sharyzhalgai Complex: more than 100 isotopic dates were obtained for its rocks by a broad spectrum of geochronologic techniques and range from 483 Ma (Petrova *et al.*, 1980) to 5760 Ma (Krylov *et al.*, 1980). These discrepancies of the geochronologic data were the reasons for various special-

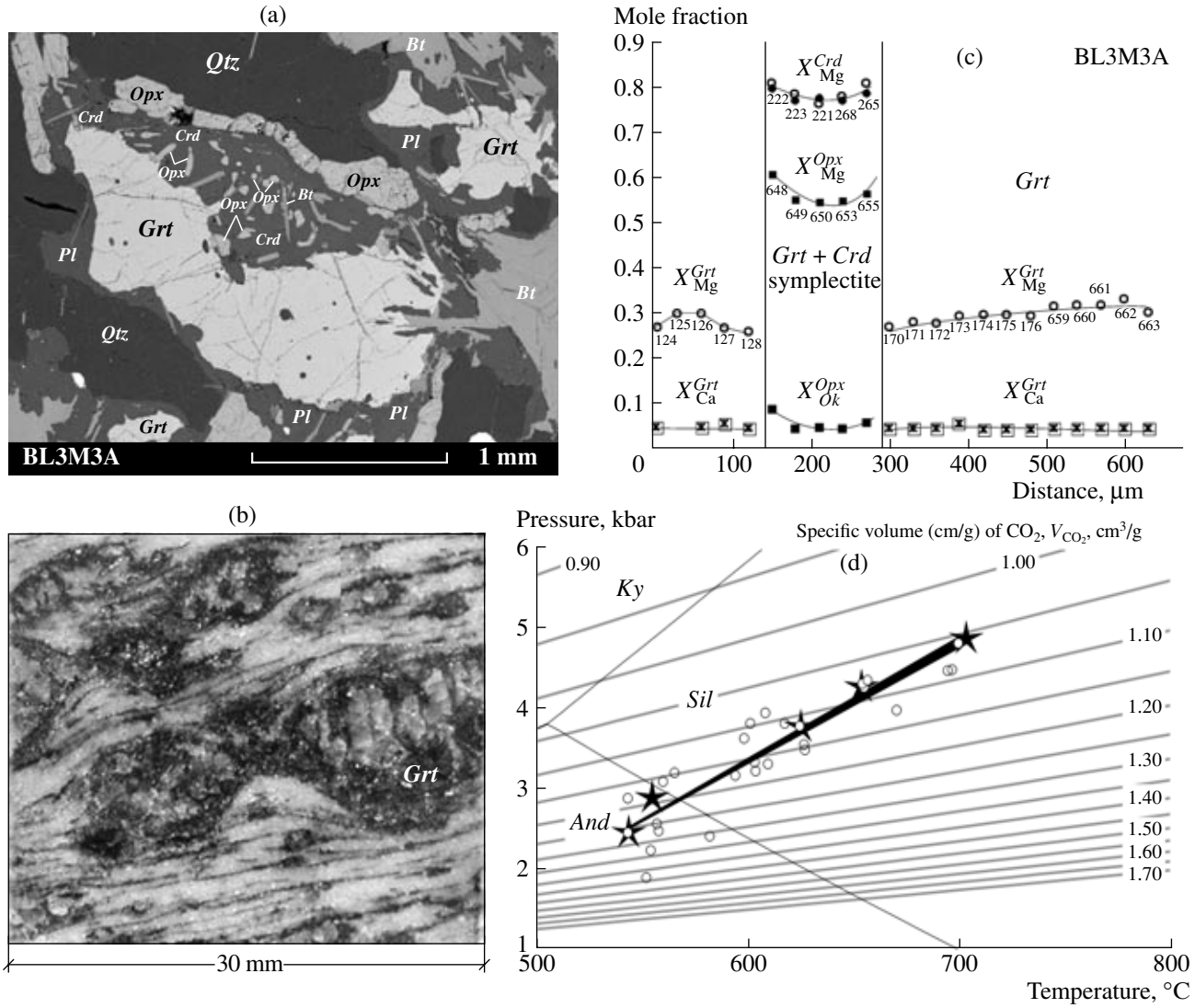

Fig. 11. Micro- and macrotexture of straight gneiss BL3M3 from the Sharyzhalgai granulite complex in the southwestern Baikal area and the *P–T* trajectory of its exhumation. (a) BSE image of a *Grt* + *Qtz* ⇒ *Opx* + *Crd* reaction texture; (b) photograph of the macrotexture of the gneiss, note that it resembles the texture of sample T73 (Fig. 9a); (c) chemical zoning of minerals; (d) *P–T* trajectory calculated based on spot microprobe analyses from Table 7. Compositional isopleths and the parameters of the local equilibrium are recalculated for $a^{fl}_{H_2O} = 0.2$.

ized structural, petrological, and geochronological studies conducted in 1983 within the scope of Project 235 of the International Geological Correlation Program. The results of this research indicate (Aftalion *et al.*, 1991; Perchuk, 1989) that the Sharyzhalgai Complex was affected by at least four major metamorphic events (Aftalion *et al.*, 1991): at 2784 +48/–45, 2467 ± 5, 1965 ± 4, and 1873 ± 4 Ma (U–Pb zircon dates). However, the section of the complex along the Lake Baikal shore displays traces of only two metamorphic stages (D2 and D3) and associated granitization (Petrova and Levitskii, 1984).

The most interesting isotopic data were obtained on the aforementioned sample of straight gneisses (sample BL3M3, Fig. 12, trajectory **II**). Zircon from this rock was dated at 2467–2497 Ma (Aftalion *et al.*, 1991). The rocks represented by this sample occur as a strongly deformed "stratum" 1.5 m thick among enderbites and mafic granulites (near 131.34 km of the Circum-Baikal Railroad). As was mentioned above, this sample shows textural features closely resembling those of metapelite sample T73 from the Central Zone of the Limpopo Complex, whose zircon age corresponds to the Late Archean (~2.6 Ga), and whose garnet was dated at 2027 ± 11 Ma (Boshoff *et al.*, 2004). By analogy, it is reasonable to suggest that the age of the last metamorphism of straight gneiss BL3M3 from the Sharyzhalgai Complex does not coincide with the zircon dates of this rocks.

Table 6. Selected microprobe analyses of minerals from *Grt* + *Qtz* ⟶ *Crd* + *Opx* reaction textures in sample BL3M3A of straight gneiss from the Sharyzhalgai granulite complex, southwestern Baikal area

Component	*Grt*	*Grt*	*Grt*	*Grt*	*Grt*	*Grt*	*Grt*	*Grt*	*Grt*	*Grt*	*Opx*	*Opx*
	EK1	EK2	EK3	EK4	EK5	EK6	EK7	EK8	EK9	EK10	EK11	EK12
SiO_2	36.85	37.23	37.58	37.69	37.00	37.51	37.01	36.87	37.11	36.57	49.68	49.66
Al_2O_3	21.07	20.80	20.54	20.58	20.74	21.03	21.29	20.94	21.01	20.92	3.01	3.36
TiO_2	0.00	0.00	0.00	0.05	0.16	0.00	0.04	0.02	0.00	0.07	0.10	0.06
Cr_2O_3	0.00	0.24	0.23	0.13	0.15	0.16	0.17	0.18	0.15	0.10	0.13	0.12
FeO*	34.12	33.97	33.65	33.55	34.16	32.94	33.36	33.90	33.85	35.83	28.37	28.04
MnO	0.84	0.67	0.93	0.74	0.88	0.88	0.76	0.85	0.81	0.57	0.17	0.17
MgO	6.19	6.02	5.73	6.30	5.86	6.39	6.42	6.26	6.12	4.87	18.50	18.27
CaO	0.78	1.00	0.93	0.94	0.81	0.99	0.95	0.85	0.87	0.99	0.01	0.15
Na_2O	0.00	0.00	0.04	0.01	0.00	0.00	0.00	0.08	0.04	0.02	0.00	0.17
K_2O	0.00	0.00	0.00	0.00	0.00	0.00	0.00	0.00	0.00	0.00	0.04	0.01
Total	99.85	99.93	99.59	99.80	99.45	99.74	99.79	99.67	99.77	99.8	100.01	100.01
Proportions of cations												
Si	2.94	2.97	3.00	3.00	2.97	2.98	2.95	2.95	2.96	2.95	1.91	1.90
Al	1.98	1.95	1.93	1.93	1.96	1.97	2.00	1.97	1.98	1.99	0.14	0.15
Ti	0.00	0.02	0.01	0.00	0.00	0.00	0.00	0.00	0.00	0.00	0.00	0.00
Cr	0.00	0.00	0.00	0.00	0.00	0.00	0.00	0.00	0.00	0.00	0.00	0.00
Fe^{2+}	2.28	2.26	2.25	2.23	2.29	2.19	2.22	2.27	2.26	2.41	0.91	0.90
Mn	0.06	0.05	0.06	0.05	0.06	0.06	0.05	0.06	0.05	0.04	0.01	0.01
Mg	0.74	0.72	0.68	0.75	0.70	0.76	0.76	0.75	0.73	0.59	1.06	1.04
Ca	0.07	0.09	0.08	0.08	0.07	0.08	0.08	0.07	0.07	0.09	0.00	0.01
Na											0.00	0.01
K											0.00	0.00
X_{Mg}	0.24	0.24	0.23	0.25	0.23	0.25	0.25	0.24	0.24	0.19	0.54	0.54
X_{Al}											0.033	0.038
X_{Ca}	0.02	0.03	0.03	0.03	0.02	0.03	0.03	0.02	0.02	0.03		
Component	*Opx*	*Crd*	*Opx*	*Opx*	*Crd*	*Crd*	*Pl*	*Pl*	*Opx*	*Crd*	*Bt*	*Bt*
	14	15	16	17	18	19	20	21	22	23	24	25
SiO_2	50.12	50.27	50.01	50.24	50.41	50.20	62.23	63.36	50.25	49.62	38.57	38.83
Al_2O_3	3.68	33.64	3.35	3.80	34.01	33.66	23.15	22.47	3.29	33.59	16.93	17.25
TiO_2	0.00	0.00	0.03	0.00	0.04	0.04	0.05	0.00	0.23	0.18	4.32	4.05
Cr_2O_3	0.30	0.10	0.36	0.21	0.04	0.00	0.00	0.04	0.18	0.14	0.51	0.49
FeO*	27.38	5.64	27.91	26.67	5.03	5.77	0.16	0.16	27.19	5.58	14.57	14.39
MnO	0.06	0.00	0.10	0.04	0.00	0.10	0.12	0.02	0.25	0.00	0.07	0.06
MgO	18.27	10.20	18.24	18.93	10.37	10.18	0.04	0.05	18.52	10.66	14.7	15.03
CaO	0.00	0.09	0.01	0.11	0.05	0.04	4.70	4.78	0.07	0.06	0.02	0.03
Na_2O	0.14	0.05	0.00	0.00	0.00	0.02	9.46	8.96	0.00	0.11	0.16	0.10
K_2O	0.04	0.00	0.00	0.00	0.05	0.00	0.08	0.16	0.00	0.07	10.15	9.78
Total	99.99	99.99	100.01	100.00	100.00	100.01	99.99	100.00	99.98	100.01	99.75	99.82
Proportions of cations												
Si	1.91	5.02	1.91	1.91	5.02	5.02	6.22	6.31	1.91	4.97	5.48	5.49
Al	0.17	3.96	0.15	0.17	3.99	3.96	2.73	2.64	0.15	3.96	2.83	2.87
Ti	0.00	0.00	0.00	0.00	0.00	0.00	0.00	0.00	0.01	0.01	0.46	0.43
Cr	0.01	0.01	0.01	0.01	0.00	0.00	0.00	0.00	0.01	0.01	0.06	0.05
Fe^{2+}	0.87	0.47	0.89	0.85	0.42	0.48	0.01	0.01	0.87	0.47	1.73	1.70
Mn	0.00	0.00	0.00	0.00	0.00	0.01	0.01	0.00	0.01	0.00	0.01	0.01
Mg	1.04	1.52	1.04	1.07	1.54	1.52	0.01	0.01	1.05	1.59	3.11	3.17
Ca	0.00	0.01	0.00	0.00	0.01	0.00	0.50	0.51	0.00	0.01	0.00	0.00
Na	0.01	0.01	0.00	0.00	0.00	0.00	1.83	1.73	0.00	0.02	0.04	0.03
K	0.00	0.00	0.00	0.00	0.01	0.00	0.01	0.02	0.00	0.01	1.84	1.76
X_{Mg}	0.54	0.76	0.54	0.56	0.79	0.76	0.31	0.36	0.55	0.77	0.64	0.65
X_{Al}	0.041		0.038	0.042					0.037			
X_{Ca}							0.21	0.23				

* All iron as FeO.

Table 7. Compositional and thermodynamic parameters of the local equilibria *Grt* + *Qtz* = *Crd* + *Opx* and *Grt* + *Qtz* + *Sil* = *Crd* for metapelites from the Sharyzhalgai granulite complex, southwestern Baikal area

Grt				*Crd*		*Opx*			*T*, °C	*P*, kbar
analytical spot	X_{Mg}	X_{Ca}	X_{Mn}	analytical spot	X_{Mg}	analytical spot	X_{Mg}	X_{Al}		
BL10J (*Grt* + *Qtz* + *Crd* + *Sil*)										
39	0.198	0.036	0.029	28	0.650				668	4.13
49	0.197	0.036	0.034	28	0.650				664	4.08
45	0.203	0.034	0.034	28	0.650				676	4.25
39	0.198	0.036	0.029	23	0.668				645	3.94
49	0.197	0.036	0.034	23	0.668				642	3.89
45	0.203	0.034	0.034	23	0.668				653	4.05
38	0.207	0.033	0.036	34	0.693				628	3.89
37	0.200	0.033	0.035	35	0.680				633	3.85
38	0.207	0.033	0.036	25	0.678				648	4.05
37	0.200	0.033	0.035	25	0.678				637	3.88
38	0.207	0.033	0.036	27	0.677				649	4.06
40	0.182	0.032	0.041	34	0.693				586	3.26
40	0.182	0.032	0.041	35	0.680				601	3.38
BL3M3 (*Grt* + *Qtz* + *Opx* + *Crd*)										
EK6	0.252	0.027	0.026	EK23	0.773	EK22	0.548	0.037	591	2.43
EK7	0.251	0.026	0.023	EK19	0.759	EK15	0.543	0.041	570	2.38
EK4	0.247	0.026	0.022	EK18	0.786	EK16	0.538	0.038	557	2.24
EK5	0.230	0.022	0.027	EK23	0.773	EK14	0.543	0.041	504	1.58
EK8	0.243	0.023	0.024	EK18	0.786	EK22	0.548	0.037	521	2.15
662	0.334	0.045	0.009	221	0.77	650	0.548	0.049	711	4.81
659	0.318	0.046	0.012	268	0.78	653	0.551	0.045	662	4.29
126	0.300	0.047	0.013	223	0.79	649	0.554	0.046	629	3.78
128	0.260	0.044	0.013	222	0.81	648	0.61	0.089	541	2.48
170	0.270	0.045	0.014	266	0.81	655	0.567	0.058	555	2.95

Indeed, a slightly rounded zircon grain shows no traces of any newly formed zones, i.e., this zircon provides no evidence of any younger metamorphic event. If so, *P–T* trajectory **II** in Fig. 12 should correspond to the event at 1.9 or even 1.81 Ga (Aftalion *et al.*, 1991). Additional support for this interpretation is provided by the paragenetic and textural features of metapelites B244 and B245: both rocks have usual granoblastic textures and occur conformably with charnockites and enderbites, which were dated at ~2.78 Ga (Aftalion *et al.*, 1991). These rocks correspond to higher pressure *P–T* path **I** in Fig. 12. It is worth noting that T_{min} = 600°C at the minimum pressure of ~4.5 kbar of this path corresponds to T_{max} = 700°C (at P_{max} ~ 4.5 kbar) for *P–T* path **II**, which was calculated for a series of rock samples with blastomylonitic textures (Fig. 12). It is reasonable to suggest that the age determined for the garnet and cordierite from these samples (possible variations from 2497 to 2467 Ma) is older that the age of the group of samples used to calculate the *P–T* trajectory **II** in Fig. 12. The difference between the age values can be as great as 800 m.y.

The thermal shift of the *P–T* trajectories shown in Fig. 12 was determined for the Sharyzhalgai Complex in the southwestern Baikal area fairly long ago (Perchuk, 1989), but no realistic explanation of this phenomenon was then proposed. At the same time, gneisses from this complex provide record of the conditions under which the ductile shear zones developed during the early stage (D2/M2) of the granulite metamorphism in the course of decompressional cooling. Also, it cannot be ruled out that the rocks can display traces of metamorphic reactions during stage D2 in rock blocks that were not strongly effected by strong repeated dynamometamorphism. This idea is supported by the find of sapphirine-bearing quartzite (sample B125) in the headwaters of the Poludennyi Toisuk

Table 8. Selected microprobe analyses of minerals from metapelite B245 with a *Grt* + *Qtz* ⟶ *Crd* + *Opx* reaction texture, Sharyzhalgai granulite complex, southwestern Baikal area

Component	19	20	23	24	25	26	30	35	42	44	45	21	28
	Grt	*Grt*	*Grt*	*Grt*	*Grt*	*Grt*	*Grt*	*Grt*	*Grt*	*Grt*	*Grt*	*Crd*	*Crd*
SiO_2	39.12	38.79	38.51	38.55	39.44	38.94	39.04	39.09	39.20	38.58	38.38	51.98	51.37
TiO_2	0.00	0.00	0.00	0.00	0.00	0.00	0.00	0.00	0.00	0.00	0.00	0.00	0.00
Al_2O_3	21.63	21.85	22.47	22.01	22.64	21.44	22.06	22.80	22.52	22.54	21.31	34.36	34.24
FeO	27.95	26.74	27.97	28.01	27.33	28.22	27.38	27.48	28.33	28.24	28.80	3.52	3.73
MnO	1.05	0.89	0.92	1.14	0.73	0.78	1.04	1.04	0.91	0.73	0.76	0.00	0.00
MgO	9.26	10.37	10.66	10.48	9.83	9.24	10.24	9.52	9.17	10.26	9.36	12.94	11.35
CaO	0.98	1.33	1.25	1.09	1.21	1.12	1.41	1.33	1.32	1.04	1.20	0.00	0.00
Na_2O	0.00	0.00	0.00	0.00	0.00	0.00	0.00	0.00	0.00	0.00	0.00	0.00	0.00
K_2O	0.00	0.00	0.00	0.00	0.00	0.00	0.00	0.00	0.00	0.00	0.00	0.00	0.00
Total	100.00	99.97	101.79	101.28	101.16	99.74	101.16	101.27	101.45	101.40	99.81	102.80	100.69
Proportions of cations													
Si	3.02	2.98	2.96	2.97	3.02	3.01	3.00	3.00	3.02	2.97	2.98	5.01	5.04
Ti	0.00	0.00	0.00	0.00	0.00	0.00	0.00	0.00	0.00	0.00	0.00	0.00	0.00
Al	1.97	1.98	1.97	1.95	1.99	1.96	1.95	2.01	1.99	1.99	1.96	3.90	3.96
Fe^{2+}	1.80	1.72	1.74	1.76	1.71	1.83	1.72	1.72	1.77	1.77	1.88	0.28	0.31
Mn	0.07	0.06	0.06	0.07	0.05	0.05	0.07	0.07	0.06	0.05	0.05	0.00	0.00
Mg	1.06	1.19	1.22	1.20	1.12	1.06	1.17	1.09	1.05	1.18	1.08	1.86	1.66
Ca	0.08	0.11	0.10	0.09	0.10	0.09	0.11	0.11	0.11	0.08	0.10	0.00	0.00
Na	0.00	0.00	0.00	0.00	0.00	0.00	0.00	0.00	0.00	0.00	0.00	0.00	0.00
K	0.00	0.00	0.00	0.00	0.00	0.00	0.00	0.00	0.00	0.00	0.00	0.00	0.00
X_{Mg}	0.37	0.41	0.41	0.41	0.40	0.37	0.41	0.39	0.37	0.40	0.37	0.87	0.84
X_{Al}	0.03	0.04	0.03	0.03	0.03	0.03	0.04	0.04	0.04	0.03	0.03	0.00	0.00
X_{Ca}	0.02	0.02	0.02	0.02	0.02	0.02	0.02	0.02	0.02	0.02	0.02	0.48	0.50
Component	34	38	41	22	27	31	32	33	37	39	5	17	18
	Crd	*Crd*	*Crd*	*Opx*	*Opx*	*Opx*	*Opx*	*Opx*	*Opx*	*Opx*	*Bt*	*Bt*	*Bt*
SiO_2	51.08	51.51	50.39	50.41	50.39	49.35	51.63	51.44	50.20	50.32	37.25	38.22	39.19
TiO_2	0.00	0.00	0.00	0.00	0.00	0.00	0.00	0.00	0.00	0.00	5.33	4.76	5.03
Al_2O_3	34.59	34.39	33.12	6.81	5.80	6.57	6.71	6.13	6.27	5.01	16.08	15.64	15.67
FeO	3.72	3.62	3.88	20.53	22.53	22.73	23.05	21.76	22.22	22.03	16.36	17.22	13.01
MnO	0.00	0.00	0.00	0.00	0.00	0.00	0.00	0.00	0.00	0.00	0.00	0.00	0.00
MgO	11.31	12.12	11.70	22.25	21.27	20.93	22.07	23.30	21.20	22.20	12.35	11.86	15.28
CaO	0.00	0.00	0.00	0.00	0.00	0.26	0.00	0.00	0.00	0.34	0.00	0.00	0.00
K_2O	0.00	0.00	0.00	0.00	0.00	0.00	0.00	0.00	0.00	0.00	10.03	9.58	9.83
Total	100.70	101.64	98.18	100.00	100.00	99.84	103.46	102.63	99.89	99.90	97.40	97.28	98.01
Proportions of cations													
Si	5.02	5.01	5.00	0.93	0.94	0.92	0.93	0.93	0.93	0.94	3.17	3.26	3.16
Ti	0.00	0.00	0.00	0.00	0.00	0.00	0.00	0.00	0.00	0.00	0.34	0.31	0.30
Al	4.00	3.95	3.94	0.15	0.13	0.14	0.14	0.13	0.14	0.11	1.61	1.57	1.49
Fe^{2+}	0.31	0.29	0.33	0.32	0.35	0.35	0.35	0.33	0.34	0.34	1.16	1.23	0.88
Mn	0.00	0.00	0.00	0.00	0.00	0.01	0.00	0.00	0.00	0.01	0.00	0.00	0.00
Mg	1.65	1.76	1.76	0.61	0.59	0.58	0.59	0.62	0.59	0.61	1.57	1.51	1.84
Ca	0.00	0.00	0.00	0.00	0.00	0.00	0.00	0.00	0.00	0.00	0.00	0.00	0.00
K	0.00	0.00	0.00	0.00	0.00	0.00	0.00	0.00	0.00	0.00	0.00	0.00	0.00
X_{Mg}	0.84	0.86	0.84	0.66	0.63	0.62	0.63	0.66	0.63	0.64	0.57	0.55	0.68
X_{Al}	0.00	0.00	0.00	0.00	0.00	0.01	0.00	0.00	0.00	0.01	0.26*	0.25*	0.24*
X_{Ca}	0.51	0.49	0.49	0.07	0.06	0.07	0.07	0.06	0.07	0.05			

Table 9. Compositional and thermodynamic parameters of local mineral equilibria in ordinary metapelite B245 from the Sharyzhalgai granulite complex, southwestern Baikal area

Grain part	*Grt*				*Crd*		*Opx*			*T*, °C	*P*, kbar
	analytical spot	X_{Mg}	X_{Ca}	X_{Mn}	analytical spot	X_{Mg}	analytical spot	X_{Mg}	X_{Al}		
core	24	0.406	0.029	0.024	calcd	0.810	31	0.621	0.072	732	5.75
core	25	0.396	0.033	0.016	calcd	0.810	31	0.621	0.072	717	5.51
core	30	0.405	0.038	0.022	calcd	0.810	31	0.621	0.072	730	5.73
core	44	0.400	0.028	0.016	calcd	0.810	31	0.621	0.072	723	5.61
margin	26	0.367	0.031	0.017	28	0.844	27	0.627	0.063	614	4.73
margin	35	0.388	0.037	0.023	34	0.844	33	0.656	0.064	638	4.89
margin	42	0.372	0.036	0.020	41	0.843	39	0.642	0.054	621	4.64
margin	20	0.409	0.036	0.019	21	0.868	33	0.656	0.064	613	5.33
margin	19	0.371	0.028	0.023	34	0.844	33	0.656	0.064	617	4.52
margin	23	0.413	0.033	0.019	34	0.844	22	0.659	0.074	669	5.45
margin	42	0.372	0.036	0.020	38	0.856	39	0.642	0.054	596	4.66
margin	1	0.325	0.038	0.025	3	0.846	8	0.614	0.065	563	3.94
margin	2	0.321	0.039	0.019	42	0.841	9	0.611	0.068	567	3.87
margin	10	0.334	0.035	0.019	11	0.847	12	0.616	0.068	571	4.13
margin	41	0.323	0.039	0.023	42	0.841	13	0.604	0.071	570	4.00

River. The rock has a fine- and medium-grained equigranular texture with large porphyroblasts of garnet surrounded by Crd_1 rims. The rock displays no traces of any older cordierite generations. Its groundmass consists of quartz, and no reaction textures develop at contacts between this mineral and garnet. The matrix of the rock contains scattered grains of *Spr*, *Grt*, *Sil*, *Bt*, and *Rt*, the cordierite rims sometimes include *Bt* and *Spl*. The garnet predominantly has the composition Grt_{30}. Garnet porphyroblasts are zonal: the cores consist of Grt_{31}, and similar values of N_{Mg}^{Grt} were determined at contacts with quartz, whereas this parameter decreases to 20–21 mol % at contacts with cordierite. The N_{Mg}^{Grt} increases from 78 mol % in the outer part of the rim to 82 mol % near contacts with $Grt_{20.5}$ and from to 84 to 85 mol % toward contacts with $Grt_{28.9}$. Selected microprobe analyses of minerals are listed in Table 10, and the *P–T* parameters of the mineral equilibria calculated from these analytical data are presented in Table 11. The *P–T* trajectory shown in Fig. 13 (heavy line) was calculated based on these data and is a continuation of trajectory **I** in Fig. 12. These *P-T* paths correspond to the exhumation of the granulites to a depth of ~15 km in the Archean (see above). However, the *P–T* path for the sapphirine gneiss implies that the rocks were uplifted at a depth of ~7 km, i.e., to a level practically equal to that recorded in sample BL3M3 (Figs. 11d, 12). In contrast to straight gneiss BL3M3, sapphirine quartzite B125 is undeformed. Hence, this rock was either produced and metamorphosed in the Early Proterozoic (1.8–1.9 Ga) or was then recrystallized under the effect of fluid somewhere outside the dynamometamorphism zone. The latter scenario seems to be more plausible, because the geologic setting of sample B125 does not imply the accumulation of sediments and their metamorphism in the Early Proterozoic. Conceivably, this problem can be solved by means of the isotopic dating of the garnet that was used to derive the *P–T* trajectory in Fig. 13, if the isotopic system of the mineral was not disturbed. After this, geodynamic models can be proposed and discussed for various evolutionary stages of the Sharyzhalgai polymetamorphic complex.

Lapland granulite complex. The age of this complex seems to provoke no doubt. Bibikova *et al.* (1993) dated (Pb–Pb) the Lapland granulite metamorphism at 1916 ± 1 to 1884 ± 18 Ma at a protolith age of ~2.2 Ga. The complex studies of various isotopic systems (U–Pb, Pb–Pb, Sm–Nd, and Rb–Sr) have not identified any older events. Moreover, Daly and Bogdanova (1991) dated garnet from granulites of the Lapland Complex at 1870 Ma (Sm–Nd method). This date seems to correspond to the youngest deformation stage of rocks under conditions of the lower granulite–upper amphibolite metamorphic facies. Hence, the isotopically dated age range of metamorphic events in the Lapland Complex was as long as 45 m.y. However,

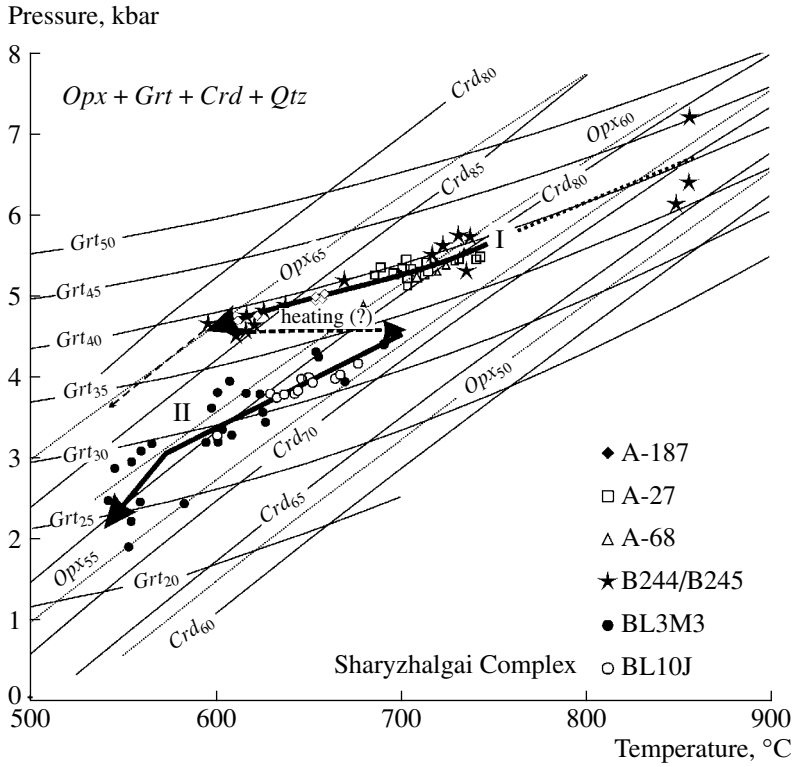

Fig. 12. *P–T* trajectories of (I) undeformed and (II) deformed gneisses from the Sharyzhalgai granulite complex in the southwestern Baikal area. The mineral assemblages (*Grt* + *Qtz* + *Crd* + *Opx* + *Bt* + *Kfs* + *Pl* + *Ap* + *Zrn*) and reaction textures (*Grt* + *Qtz* ⇒ *Crd* + *Opx*) in all of the samples (A-187, A-27, A-68, B245, BL3M3, and BL10J) are analogous. Trajectory **II** is supposedly related to repeated high-temperature metamorphism in ductile shear zones during exhumation. See Tables 6 and 8 for selected microprobe analyses and Tables 7 and 9 for compositional and thermodynamic parameters. The reader can find data on the other samples in (Gerya, 1999).

detailed information on the geologic structure and the structural–textural characteristics of the dated rocks were not described in the aforementioned papers.

The results of detailed petrological studies make it possible to reproduce, at least partly, the thermal and dynamic history of the Lapland granulite complex. For example, Raith and Raase (1986) recognized two high-grade metamorphic stages: (1) M1 ($T \sim 850$°C, $P \sim 8$ kbar, and $\mu_{CO_2}^{fl} > 0.8$) in the presence of a CO_2-rich fluid and (2) postkinematic M2 ($T = 830$–760°C, $P = 7.2$–6.2 kbar, and $\mu_{CO_2}^{fl} = 0.9$–0.6). These stages are described by trajectory *1* in Fig. 14b, which was calculated by Fonarev *et al.* (1994). This *P–T* trajectory is identical to *P–T* trajectory *3* for metapelite of the Kola Group (sample KL1098; Gerya, 1999): in Fig. 14b, *P–T* trajectory *3* practically coincides with the subisobaric segment of *P–T* path *1*. Fonarev *et al.* (1994) have also calculated a high-pressure *P–T* path for metabasalts of the Lapland Complex (Fig. 14b, trajectory *2*), which enters the kyanite stability field. This *P–T* path reflects the exhumation of the rocks from the lower crust (~12 kbar) and their crystallization in the middle part of the continental crust (6.4 kbar). Analyses of locally equilibrated minerals in metapelite gneiss Lg34 from the northern part of the complex were used to calculate higher temperature but lower pressure *P–T* path *4* (Fig. 14b). Detailed descriptions of this and other metapelites and numerous microprobe analyses of their locally equilibrated minerals were published in (Gerya, 1999). Some compositional and thermodynamic parameters of mineral equilibria in these rocks are listed in Table 12.

The diagram in Fig. 14b summarizes data on the thermal and dynamic history of the Lapland Complex. The *P–T* paths in Fig. 14b were not dated isotopically, but this diagram clearly demonstrates that the first metamorphic stage has terminated in the middle part of the crust supposedly at ~1.92 Ga (Bibikova *et al.*, 1993). It cannot be ruled out that a few dozen million years later, perhaps, at ~1.88 Ga, the rocks were reheated in dynamometamorphic zones, and the whole complex was exhumed into the upper crust. Obviously, the repeated metamorphism could not occur without inflow of fluids and their active participation in the evolution of the Lapland Complex. Fonarev and Kreulen (1995) utilized data on fluid inclusions in minerals of

Table 10. Selected microprobe analyses of minerals from metapelite B125 with a *Grt* + *Qtz* + *Sil* ⟶ *Crd* reaction texture, Sharyzhalgai granulite complex, southwestern Baikal area

Component	13	14	15	16	20	23	24	25	30	31	33	34	35
	Grt	*Grt*	*Grt*	*Grt*	*Grt*	*Grt*	*Grt*	*Grt*	*Grt*	*Grt*	*Grt*	*Grt*	*Grt*
SiO_2	37.95	37.4	37.29	37.19	37.12	37.18	38.14	37.66	37.06	37.32	37.31	37.94	37.52
TiO_2	0	0	0	0	0	0	0	0	0	0	0	0	0
Al_2O_3	21.89	21.74	21.18	21.97	21.4	21.87	21.48	21.46	21.6	20.99	21.35	21.57	21.23
FeO	31.94	32.21	32.82	33.19	33.66	31.54	30.99	32.55	32.2	31.86	30.89	31.57	31.16
MnO	1.04	0.89	1.11	0.9	1.01	0.84	0.98	0.81	1.03	1	0.62	0.83	0.94
MgO	7.31	7.3	6.12	6.04	5.83	7.56	7.29	6.7	6.64	6.55	7.61	7.66	7.11
CaO	0.4	0.43	0.4	0.51	0.51	0.51	0.46	0.4	0.46	0.35	0.49	0.62	0.48
Na_2O	0.00	0.00	0.00	0.00	0.00	0.00	0.00	0.00	0.00	0.00	0.00	0.00	0.00
K_2O	0.00	0.00	0.00	0.00	0.00	0.00	0.00	0.00	0.00	0.00	0.00	0.00	0.00
Proportions of cations													
Si	2.97	2.95	2.98	2.95	2.96	2.94	3.00	2.98	2.96	3.00	2.97	2.97	2.99
Ti	0.00	0.00	0.00	0.00	0.00	0.00	0.00	0.00	0.00	0.00	0.00	0.00	0.00
Al	2.02	2.02	2.00	2.05	2.01	2.04	1.99	2.00	2.03	1.99	2.01	1.99	1.99
Fe^{2+}	2.09	2.12	2.20	2.20	2.25	2.08	2.04	2.15	2.15	2.14	2.06	2.07	2.08
Mn	0.07	0.06	0.08	0.06	0.07	0.06	0.07	0.05	0.07	0.07	0.04	0.06	0.06
Mg	0.85	0.86	0.73	0.71	0.69	0.89	0.86	0.79	0.79	0.78	0.90	0.89	0.84
Ca	0.03	0.04	0.03	0.04	0.04	0.04	0.04	0.03	0.04	0.03	0.04	0.05	0.04
X_{Mg}	0.29	0.29	0.25	0.24	0.24	0.30	0.30	0.27	0.27	0.27	0.31	0.30	0.29
X_{Ca}	0.02	0.02	0.02	0.02	0.02	0.02	0.02	0.02	0.02	0.02	0.02	0.48	0.50
Component	17	18	21	22	26	27	32	36	37	40	64	77	88
	Crd	*Crd*	*Crd*	*Crd*	*Crd*	*Crd*	*Crd*	*Crd*	*Crd*	*Crd*	*Crd*	*Crd*	*Crd*
SiO_2	47.93	48.88	48.34	48.54	47.61	48.76	46.88	49.12	48.16	49.59	37.25	38.22	39.19
TiO_2	0.00	0.00	0.00	0.00	0.00	0.00	0.00	0.00	0.00	0.00	5.33	4.76	5.03
Al_2O_3	32.99	33.48	33.26	33.22	33.08	33.09	32.18	32.79	33.16	33.55	16.08	15.64	15.67
FeO	4.05	4.06	3.60	4.30	3.56	4.29	3.64	3.68	3.74	3.47	16.36	17.22	13.01
MnO	0.00	0.00	0.00	0.00	0.00	0.00	0.00	0.00	0.00	0.00	0.00	0.00	0.00
MgO	11.62	11.20	11.39	11.56	11.52	11.48	11.40	11.50	11.24	11.85	12.35	11.86	15.28
CaO	0.00	0.00	0.00	0.00	0.00	0.00	0.00	0.00	0.00	0.00	0.00	0.00	0.00
Proportions of cations													
Si	4.93	4.97	4.96	4.95	4.93	4.97	4.94	5.01	4.96	4.99	4.74	5.14	4.96
Ti	0.00	0.00	0.00	0.00	0.00	0.00	0.00	0.00	0.00	0.00	0.00	0.00	0.00
Al	4.00	4.01	4.02	3.99	4.04	3.97	4.00	3.94	4.02	3.97	4.36	3.84	3.98
Fe^{2+}	0.35	0.35	0.31	0.37	0.31	0.37	0.32	0.31	0.32	0.29	0.36	0.33	0.35
Mn	0.00	0.00	0.00	0.00	0.00	0.00	0.00	0.00	0.00	0.00	0.00	0.00	0.00
Mg	1.78	1.70	1.74	1.76	1.78	1.74	1.79	1.75	1.72	1.77	1.61	1.64	1.77
Ca	0.00	0.00	0.00	0.00	0.00	0.00	0.00	0.00	0.00	0.00	0.00	0.00	0.00
X_{Mg}	0.84	0.83	0.85	0.83	0.85	0.83	0.85	0.85	0.84	0.86	0.82	0.83	0.84

Table 11. Compositional and thermodynamic parameters of local mineral equilibria in sapphirine quartzite B125 from the Sharyzhalgai granulite complex, southwestern Baikal area

Grain part	*Grt*				*Crd*		*T*, °C	*P*, kbar
	analytical spot	X_{Mg}	X_{Ca}	X_{Mn}	analytical spot	X_{Mg}		
core	13	0.290	0.011	0.023	22	0.827	558	4.06
core	14	0.288	0.012	0.019	18	0.831	550	3.98
core	33	0.305	0.014	0.014	37	0.843	549	4.13
core	34	0.302	0.017	0.018	37	0.843	546	4.08
core	23	0.299	0.014	0.018	27	0.827	569	4.22
core	24	0.295	0.013	0.022	27	0.827	564	4.15
core	43	0.305	0.013	0.021	37	0.843	549	4.13
core	84	0.235	0.017	0.023	22	0.827	496	3.08
core	85	0.266	0.013	0.026	22	0.827	531	3.64
core	52	0.290	0.015	0.020	37	0.843	533	3.88
core	53	0.295	0.016	0.027	37	0.843	538	3.96
core	72	0.255	0.011	0.022	63	0.777	589	3.97
core	73	0.246	0.014	0.019	63	0.777	577	3.79
core	76	0.234	0.008	0.022	77	0.833	487	3.01
margin	80	0.221	0.011	0.027	77	0.833	472	2.78
margin	87	0.242	0.011	0.023	88	0.836	491	3.13
margin	15	0.249	0.012	0.025	17	0.836	499	3.25
margin	16	0.245	0.015	0.020	17	0.836	495	3.18
margin	25	0.268	0.011	0.018	26	0.852	495	3.41
margin	30	0.269	0.013	0.023	32	0.848	503	3.47
margin	31	0.268	0.010	0.023	32	0.848	502	3.45
margin	38	0.264	0.017	0.017	40	0.859	481	3.27
margin	39	0.266	0.016	0.018	40	0.859	483	3.31
margin	35	0.289	0.014	0.021	36	0.848	524	3.81
margin	44	0.289	0.016	0.028	45	0.855	512	3.72
margin	48	0.258	0.013	0.019	47	0.847	493	3.3
margin	49	0.273	0.017	0.018	47	0.847	508	3.55
margin	51	0.275	0.014	0.025	50	0.855	498	3.49
margin	54	0.214	0.010	0.023	55	0.819	482	2.76
margin	57	0.212	0.010	0.026	56	0.799	505	2.89
margin	58	0.224	0.015	0.027	56	0.799	520	3.13
margin	20	0.236	0.015	0.022	21	0.849	467	2.9
margin	65	0.208	0.009	0.027	64	0.817	478	2.67
margin	66	0.204	0.011	0.021	64	0.817	473	2.59

various rocks from this complex to demonstrate that it has been metamorphosed in a number of stages.

Note *P–T* path *3* in Fig. 14b, which was calculated for Late Archean metapelite KL1098 from the Kola Group (Fig. 14c). As was mentioned above, this *P–T* trajectory coincides with subisobaric *P–T* trajectory *1* and demonstrates the *P–T* parameters at which the reaction textures $Grt_1 + Qtz = Crd_1 + Opx$ grew (Fig. 14d), and the T_{min} of this trajectory corresponds to the T_{max} of trajectory *5*. This suggests subisobaric heating (*P–T*

trajectory *4*). If isotopic geochronologic data can be found that will support this hypothetic *P–T* path segment, then the Lapland granulite complex (~1.9 Ga) can turn out to be the product of the repeated high-temperature metamorphism of the Kola Group granulites (~2.6–2.7 Ga). This is consistent with currently existing concepts concerning the evolution of the Lapland granulites (Mints *et al.*, 1996; Bibikova *et al.*, 1993). However, the aforementioned information on the metamorphic regimes still does not allow the reconstruction of the chronology of metamorphic events in the Lapland Complex before its exhumation.

CONCLUSIONS

In order to elucidate the thermal and dynamic evolution of granulite complexes, particularly those affected by polymetamorphism, the researcher should devote much attention to ductile shear zones that consist of straight gneisses. The latter are massive rocks with clearly pronounced linear gneissosity and a blastomylonitic structure. These rocks often grade into augen gneisses and could be produced by (1) the primary exhumation of metamorphic complexes and/or (2) by overprinted high-temperature metamorphism. The configurations of the *P–T* trajectories of these rocks make it possible to distinguish between these mechanisms. Ductile shear zones developed in Archean granulite complexes simultaneously with the exhumation of these complexes, and, thus, the *P–T* paths of the corresponding straight gneisses are parts of the *P–T* trajectories of decompressional or isobaric cooling. The straight gneisses of Proterozoic zones of high-temperature ductile deformations overprinted onto Archean granulite complexes have Z-shaped configurations of their *P–T* trajectories. This implies that, under a constant pressure in the middle continental crust, the T_{min} of the older *P–T* trajectory corresponds to the T_{max} of the younger trajectory, and often $T_{max} - T_{min} > 100°C$. These zones commonly have en echelon morphologies in structural geological maps and can cut Archean gneisses, exerting no significant thermal effect on the reequilibration of their minerals near contacts. This does not rule out the possibility of fluid infiltration through Archean gneisses outside ductile shear zones. In this situation, the texture of the rock remains granoblastic, but its minerals become re-equilibrated on the continuation of the Archean *P–T* trajectory. Such relations were also identified in the granulite complexes of Limpopo in South Africa, Sharyzhalgai in the southwestern Baikal area, and Lapland in the Kola Peninsula. The origin of young ductile shear zones is demonstrated to have been caused not only by tectonic processes but also by the inflow of fluids (Hisada *et al.*, 2005). The Proterozoic *P–T* paths of these complexes

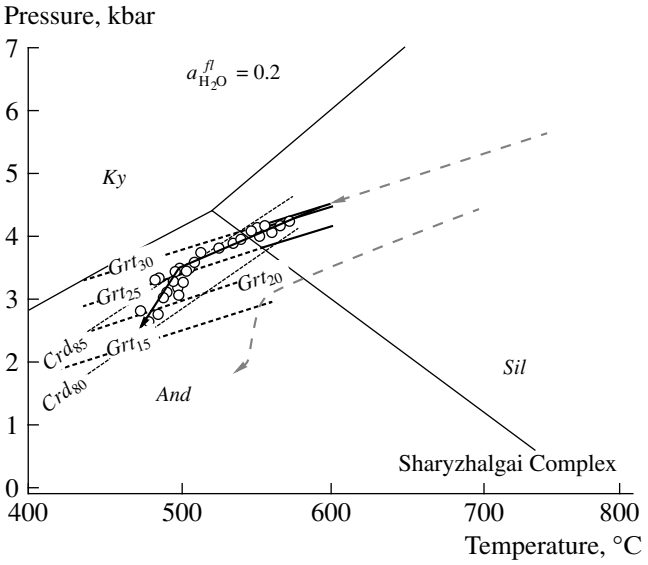

Fig. 13. *P–T* trajectory for undeformed sapphirine-bearing quartzite (sample B125) from the Sharyzhalgai granulite complex in the southwestern Baikal area. The diagram demonstrates that the *P–T* trajectory recorded in mineral equilibria in this rock is a continuation of the *P–T* trajectory for samples B244 and B245, but the absence of ductile deformations from this quartzite suggest that its minerals were re-equilibrated during the exhumation of the rock outside dynamometamorphism zones but simultaneously with their development (see, for example, sample BL3M3 in Fig. 11). See Table 10 for the analytical data. The compositional isopleths and *P–T* parameters of the *Sil* + *Grt* + *Qtz* ⇒ *Crd* local equilibrium were calculated at $a^{fl}_{H_2O}$ = 0.2. The *P–T* trajectories shown as dashed lines with arrows are the same as in Figs. 11 and 12.

are continuations of their Archean trajectories of decompressional or isobaric cooling.

The age relations along the *P–T* trajectories of the Sharyzhalgai and Lapland complexes were determined only indirectly, on the basis of the comparative analysis of similar phenomena and processes in the Limpopo granulite belt. At the same time, both complexes display isotopic and structural traces of a repeated high-temperature metamorphism. It is necessary to demonstrate by means of structural mapping that the straight gneisses are spatially restricted to certain zones of ductile deformations, to isotopically date mineral participating in reactions (5) and (7), and also try to determine the isotopic age of the marginal portions of zircon grains from metapelites in the northern part of the complex (near the Finnish boundary). Sample Lg34, whose *P–T* trajectory is displayed in Fig. 14b, was taken in this part of the complex.

The results of our research provide insight in the reasons for the significant discrepancies between the isotopic ages in HT–HP polymetamorphic complexes. The most significant results can be obtained by means

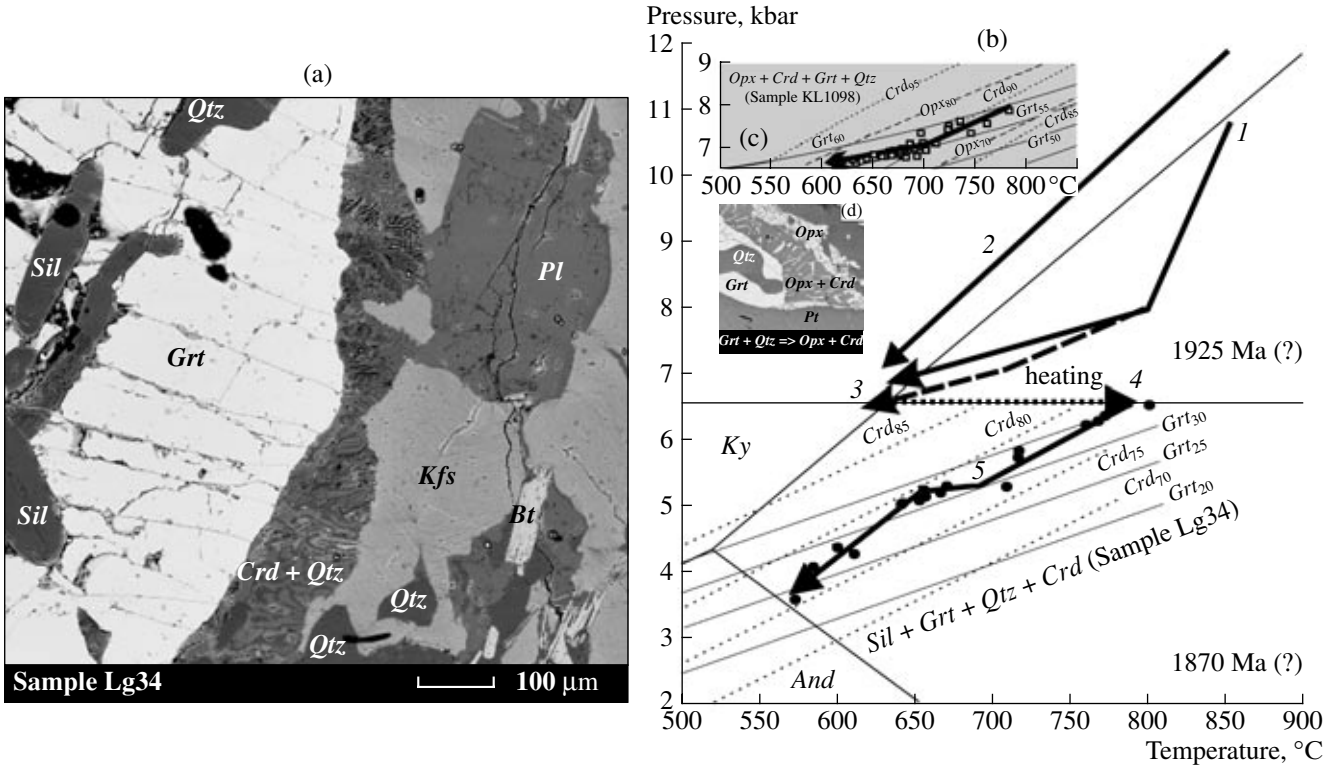

Fig. 14. (a) Microtexture of sample Lg34 from the northern inner contact zone of the Lapland granulite complex (near the boundary of Finland) and (b) *P–T* trajectories for the exhumation of the granulites of this complex (Early Proterozoic) and the Kola Group (sample KL1098, Late Archean). (a) BSE image demonstrating that garnet from sample Lg34 is elongated (pencil garnet) and was in equilibrium with *Sil*, *Qtz*, *Bt*, and *Kfs* but is replaced by *Crd* + *Qtz* symplectite. (b) *P–T* trajectories: *1* and *2* correspond to the exhumation of the Lapland Complex, according to (Fonarev *et al.*, 1994); *3* is the *P–T* trajectory for sample KL1098 (Kola Group) calculated based on the data of Table 12 and coinciding with *P–T* trajectory *2* and the parameters evaluated in (Raith and Haase, 1986); *4* is the hypothetical *P–T* trajectory of isobaric heating at ~1.91 Ga; *5* is the *P–T* trajectory derived for metapelite Lg34 (Table 12) from the northern contact zone of the Lapland Complex with the Inari greenstone belt. The exhumation of the Lapland Complex from the lower crust (~12 kbar) into the middle crust (~6.4 kbar) supposedly took place at 1916 ± 1 Ma (Bibikova *et al.*, 1993). Figure 14b demonstrates that the P_{min} of trajectory *5* coincides with the P_{max} of trajectory *2*, but the temperature at the beginning of trajectory *5* is much higher. This suggests that the rock heating (trajectory *4*) in the middle part of the continental crust and their subsequent exhumation occurred no later than 1870 Ma (Daly and Bogdanova, 1990). Sample KL1098 (*P–T* trajectory *3*) was taken from the Kola Group of Late Archean age. *P–T* trajectory *3* (Fig. 14c) corresponds to the development of the reaction texture *Grt* + *Qtz* ⇒ *Crd* + *Opx* (Fig. 14d), and its T_{min} corresponds to the T_{max} of *P–T* trajectory *5* in Fig. 14b. This also implies subisobaric heating (trajectory *4*). If so, the Lapland granulite complex (~1.9 Ga) was produced by the repeated high-temperature metamorphism of the Late Archean (~2.6 Ga) granulites of the Kola Group (Bibikova *et al.*, 1993; Mints *et al.*, 1996).

of complex (isotopic geochronological, structural geological, and detailed petrological) examination of granulites with the calculation of their *P–T* trajectories. The widely used method of zircon dating proves to be not always efficient enough: even straight metapelitic gneisses completely recrystallized in ductile shear zones can preserve zircon whose Archean isotopic systematics remain undisturbed even in the outermost zones (see, for example, Bibikova *et al.*, 1993; Boshoff *et al.*, 2004). In this context, it can turn out that efficient geochronologic tools may be silicate mineral (garnet, cordierite, sillimanite, and others) that participated in reactions during various evolutionary stages of the rocks and that were used to calculate the *P–T* paths (if the isotopic systems of these minerals remain undisturbed, and the minerals themselves were carefully selected with subsequent enrichment of the studied mineral in radiogenic elements by several stages of acid leaching). An example of this type is the very accurately determined isotopic age of garnet from granulite from the Limpopo Complex (van Reenen *et al.*, 2004). This does not rule out the possibility of using zircon ages in situations when the geological relations of granite veinlets make it possible to unambiguously distinguish between D3 and D2 zones. The two problems related to HT–HP metamorphism are quite obvious: thermodynamic and geochronologic. This implies that the configurations of *P–T* paths should be used to identify the heat sources and mechanisms responsible for the exhumation of the rocks from the lower to middle crust, as well as to date discrete stages of these process. The former problem is related to the problem of rock

Table 12. Compositional and thermodynamic parameters of mineral equilibria in metapelites from the Lapland granulite complex (analytical data from Perchuk *et al.*, 1999)

Sample Lg34 (*Crd* + *Grt* + *Sil* + *Qtz* + *Bt*)								Sample KL1098 (*Grt* + *Qtz* + *Qpx* + *Crd*)										
	Grt			*Crd*		*T*, °C	*P*, kbar		*Grt*			*Opx*			*Crd*		*T*, °C	*P*, kbar
grain part	analytical spot	X_{Ca}	X_{Mg}	analytical spot	X_{Mg}			grain part	analytical spot	X_{Ca}	X_{Mg}	analytical spot	X_{Mg}	X_{Al}	analytical spot	X_{Mg}		
core	115	0.027	0.346	89	0.745	776	6.39	core	1	0.572	0.010	52	0.749	0.060	53	0.887	762	7.62
core	103	0.029	0.342	91	0.774	715	5.82	core	1	0.572	0.010	58	0.755	0.061	61	0.898	724	7.48
core	104	0.028	0.341	91	0.774	714	5.80	core	1	0.572	0.010	30	0.731	0.067	31	0.881	783	7.90
core	105	0.026	0.348	90	0.753	763	6.28	core	1	0.572	0.010	28	0.738	0.063	29	0.895	735	7.68
core	106	0.028	0.355	90	0.753	774	6.44	core	2	0.561	0.009	52	0.749	0.060	53	0.887	746	7.40
core	107	0.026	0.361	89	0.745	800	6.72	core	2	0.561	0.009	73	0.746	0.073	72	0.902	697	7.40
core	108	0.027	0.353	90	0.753	771	6.40	margin	33	0.540	0.007	36	0.774	0.066	37	0.917	621	6.63
core	6	0.029	0.283	11	0.723	712	5.30	margin	33	0.540	0.007	48	0.733	0.073	49	0.897	687	7.15
margin	99	0.026	0.323	97	0.799	645	5.08	margin	33	0.540	0.007	50	0.745	0.063	51	0.892	701	6.99
margin	98	0.025	0.324	97	0.799	646	5.10	margin	33	0.540	0.007	25	0.732	0.065	26	0.899	680	7.03
margin	100	0.025	0.322	96	0.789	660	5.19	margin	34	0.533	0.006	36	0.774	0.066	37	0.917	614	6.51
margin	101	0.028	0.317	93	0.787	656	5.12	margin	34	0.533	0.006	38	0.756	0.067	39	0.917	615	6.66
margin	102	0.029	0.319	92	0.781	670	5.24	margin	34	0.533	0.006	40	0.740	0.063	41	0.895	683	6.84
margin	109	0.027	0.319	92	0.781	670	5.25	margin	34	0.533	0.006	46	0.736	0.069	47	0.889	702	7.00
margin	110	0.026	0.329	93	0.787	673	5.36	margin	34	0.533	0.006	48	0.733	0.073	49	0.897	678	6.96
margin	111	0.026	0.334	97	0.799	660	5.29	margin	34	0.533	0.006	50	0.745	0.063	51	0.892	693	6.86
margin	9	0.029	0.265	8	0.769	614	4.31	margin	35	0.539	0.013	36	0.774	0.066	37	0.917	620	6.61
margin	34	0.028	0.283	33	0.792	605	4.41	margin	90	0.552	0.009	111	0.753	0.061	109	0.904	678	7.01
margin	65	0.028	0.266	64	0.788	588	4.12	margin	92	0.546	0.010	96	0.778	0.066	97	0.915	634	6.70
margin	9	0.032	0.225	8	0.756	576	3.60	margin	92	0.546	0.010	102	0.760	0.069	103	0.910	652	6.90
margin	13	0.033	0.220	12	0.772	550	3.36	margin	92	0.546	0.010	107	0.755	0.073	105	0.902	677	6.98

heating in the middle crust due to internal viscous friction (Burg and Gerya, 2005; Perchuk, 2005). The other problem is more complicated. On the one hand, it is related to the distortion of an early (for example, Archean) isotopic system under the very weak effect of overprinted high-temperature metamorphism (of, for example, Proterozoic age). On the other hand, this problem is related to the possibility of incomplete reequilibration of the isotopic systems in minerals during this metamorphism (see, for example, Boshoff *et al.*, 2006).

ACKNOWLEDGMENTS

The authors thank O.V. Avchenko (Far East Geological Institute, Far East Division, Russian Academy of Sciences), E.V. Bibikova (Vernadsky Institute of Geochemistry and Analytical Chemistry, Russian Academy of Sciences), and V.V. Reverdatto (Institute of Mineralogy and Petrography, Siberian Division, Russian Academy of Sciences) for reviewing the manuscript and for valuable comments. S.P. Korikovsky (Institute of the Geology of Ore Deposits, Petrography, Mineralogy, and Geochemistry, Russian Academy of Sciences) and F.A. Letnikov (Institute of the Earth's Crust, Siberian Division, Russian Academy of Sciences) are thanked for discussing the manuscript. This study was financially supported by the Russian Foundation for Basic Research (project nos. 02-05-64025, 03-15-64633, and 04-05-64896) and the Program of the President of the Russian Federation "Leading Research Schools of Russia" (NSH 1645.2003.5, head of the school L.L. Perchuk).

REFERENCES

1. M. Aftalion, E. V. Bibikova, D. R. Bowes, *et al.*, "Timing of Early Proterozoic Collisional and Extensional Events in the Granulite–Gneiss–Charnockite–Granite Complex, Lake Baikal, USSR: A U–Pb, Rb–Sr, and Sm–Nd Study," J. Geol. **99**, 851–862 (1991).

2. L. Y. Aranovich and K. K. Podlesskii, "Geothermobarometry of High-Grade Metapelites: Simultaneously Operating Reactions," in *Evolution of Metamorphic Belts*, Ed. by J. S. Daly, B. W. D. Yardley, and B. R. Cliff, Geol. Soc. London Spec. Publ. **42**, pp. 41–65 (1989).
3. L. Ya. Aranovich and N. A. Kosyakova, "Experimental Study of the Cordierite = Orthopyroxene + Quartz Equilibrium in the FeO–MgO–Al_2O_3–SiO_2 System," Dokl. Akad. Nauk SSSR **274** (2), 399–401 (1984).
4. L. Ya. Aranovich, *Mineral Equilibria of Multicomponent Solid Solutions* (Nauka, Moscow, 1991) [in Russian].
5. R. A. Armstrong, W. Compston, and E. A. Retief, "Zircon Ion Microprobe Studies Bearing on the Age and Evolution of the Witwatersrand Triad," Precambrian Res. **53**, 243–256 (1991).
6. H. Austrheim and W. Griffin, "Shear Deformation and Eclogite Formation within Granulite-Facies Anorthosites of the Bergen Arcs, Western Norway," Chem. Geol. **50**, 267–281 (1985).
7. H. Austrheim, "The Granulite–Eclogite Facies Transition: A Comparison of Experimental Work and a Natural Occurrence in the Bergen Arcs, Western Norway," Lithos **25**, 163–169 (1990).
8. S. L. Baldwin, B. D. Monteleone, L. E. Webb, *et al.*, "Pliocenic Eclogite Exhumation at Plate Tectonic Rates in Eastern Papua New Guinea," Nature **431**, 264–267 (2004).
9. N. V. Berdnikov, *Fluid and Melt Inclusions in Precambrian Metamorphic Complexes of Russian Far East* (Nauka, Moscow, 1987) [in Russian].
10. E. V. Bibikova, V. F. Mel'nikov, and K. Kh. Avakyan, "Lapland Granulites: Petrology, Geochemistry, and Isotope Age," Petrologiya **1** (2), 215–234 (1993).
11. *Biotite–Garnet–Cordierite Equilibria and Metamorphic Evolution* (Nauka, Moscow, 1983) [in Russian].
12. R. Boshoff, C. A. Smit, D. D. van Reenen, *et al.*, "Geological History of the Central Zone of the Limpopo Complex," J. Geol. (in press).
13. R. Boshoff, D. D. van Reenen, C. A. Smit, *et al.*, "New Data Linking Major Fold Types in the Central Zone of the Limpopo Complex to Distinct Tectono-Metamorphic Events," in *Proceedings of Geoscience Africa, Johannesburg, South Africa, 2004* (Witwatersrand Univ., Johannesburg, 2004), pp. 76–77.
14. J. P. Bush, E. J. Essin, and B. A. van der Pluijim, "Evolution of Deep-Crustal Normal Faults: Constraints from Thermobarometry in the Grenville Orogen, Ontario, Canada," Tectonophysics **265**, 83–100 (1995).
15. A. Camacho, J. K. W. Lee, B. J. Hensen, *et al.*, "Short-Lived Orogenic Cycles and the Eclogitization of Cold Crust by Spasmodic Hot Fluids," Nature **435**, 1191–1196 (2005).
16. C. J. Carson, R. Powell, and G. L. Clark, "Calculated Mineral Equilibria for Eclogites in the CaO–Na_2O–FeO–MgO–Al_2O_3–SiO_2–H_2O System: Application to the Pouébo Terrane, Pam Peninsula, New Caledonia," J. Metamorph. Geol. **17**, 9–24 (1999).
17. S. Daly and S. Bogdanova, "Timing of the Metamorphism in the Lapland Granulite Belt, Finland," Res. Terrae Ser. A, No. 5, 11 (1991).
18. A. Davidson, "Identification of Ductile Shear Zones in the Southwestern Grenville Province of the Canadian Shield," in *Precambrian Tectonics Illustrated*, Ed. by A. Kroner and R. Greilig (E. Schweizerbartische Verlagsbuchhandlung (Nogöle Obermiller), Stuttgardt, 1984a), pp. 263–279.
19. A. Davidson, "Tectonic Boundaries within the Grenville Province of the Canadian Shield," J. Geodynam. **1**, 433–444 (1984b).
20. J. B. Dawson, S. L. Harley, and R. L. Rudnick, "Equilibration and Reaction in Archaean Sapphirine Granulite Xenoliths from the Lace Kimberlite Pipe, South Africa," J. Metamorph. Geol. **15**, 253–266 (1997).
21. M. J. de Wit, C. Roering, R. J. Hart, *et al.*, "Formation of an Archean Continent," Nature **357**, 553–562 (1992).
22. H. C. Dortland, N. J. Beukes, and J. Gutzmer, "Trends in Detrital Zircon Provenance from Neoarchean–Paleoproterozoic Sedimentary Successions of the Kaapvaal Craton," in *Proceedings of Geoscience Africa, Johannesburg, South Africa, 2004* (Witwatersrand Univ., Johannesburg, 2004), pp. 176–177.
23. V. I. Fonarev and R. Kreulen, "Polymetamorphism in the Lapland Granulite Belt: Evidence from Fluid Inclusions," Petrologiya **3** (4), 379–396 (1995).
24. V. I. Fonarev, "Metamorphic Evolution of the Kolvitsa Anorthosite Massif (Lapland–Kolvitsa Granulite Belt, Baltic Shield)," Dokl. Akad. Nauk **395** (3), 397–402 (2003) [Trans. Russ. Acad. Sci., Earth Sci. Sec. **395A** (3), 364 (2003)].
25. V. I. Fonarev, A. A. Grafchikov, and A. N. Konilov, "Experimental Study of Equilibria with Minerals of Variable Composition and Geological Thermobarometry," in *Experimental Problems in Geology* (Nauka, Moscow, 1994), pp. 323–355 [in Russian].
26. V. I. Fonarev, A. N. Konilov, and A. T. Rao, "*P–T* Conditions of Polymetamorphism in the Central Part of the Eastern Ghats Mobile Belt, India," Petrologiya **6** (1), 79–95 (1998) [Petrology **6** (1), 70 (1998)].
27. B. R. Frost and T. Chacko, "The Granulite Uncertainty Principle: Limitations on Thermobarometry in Granulites," J. Geol. **97**, 435–450 (1989).
28. T. V. Gerya and B. Stoeckhert, "Exhumation Rates of High Pressure Metamorphic Rocks in Subduction Channels: the Effect of Rheology," Geophys. Res. Lett. **29** (8), 102-1–102-4 (2002).
29. T. V. Gerya and L. L. Perchuk, "A New Thermodynamic Database GEOPATH for Thermobarometry," in *Proceedings of 16th Meeting of International Mineralogical Association, Pisa, Italy, 1994* (Pisa, 1994), p. 142.
30. T. V. Gerya and L. L. Perchuk, "Equations of State of Compressed Gases for Thermodynamic Databases Used in Petrology," Petrologiya **5** (4), 412–427 (1997) [Petrology **5** (4), 366 (1997)].
31. T. V. Gerya and L. L. Perchuk, "GEOPATH: a New Computer Program for Geothermobarometry and Related Calculations with the IBM PC Computer," in *Proceedings of the 15th Meeting of International Mineralogical Association, Beijing, China, 1990* (Beijing, 1990), Vol. 2, p. 1010.
32. T. V. Gerya and L. L. Perchuk, "GEOPATH—A Thermodynamic Database for Geothermobarometry and Related Calculations with the IBM PC Computer," in

Proceedings of 29th International Geological Congress, Kyoto, Japan, 1992 (Kyoto, 1992), Vol. 2, p. 1026.

33. T. V. Gerya and W. V. Maresch, "Metapelites of the Kanskiy Granulite Complex: Kinked *P–T* Path and Geodynamic Model," J. Petrol. **45** (2), 1393–1412 (2004).
34. T. V. Gerya, "Method of Physicochemical Simulation of Metamorphic Reactions Using Mass-Balance Conditions," in *Contributions to Physicochemical Petrology* (Nauka, Moscow, 1991), Vol. 16, pp. 112–127 [in Russian].
35. T. V. Gerya, B. Stoeckhert, and A. L. Perchuk, "Exhumation of High-Pressure Metamorphic Rocks in a Subduction Channel: a Numerical Simulation," Tectonics **21** (6), 6-1–6-19 (2001).
36. T. V. Gerya, Doctoral Dissertation in Geology and Mineralogy (MGU, Moscow, 1999).
37. T. V. Gerya, K. K. Podlesskii, L. L. Perchuk, *et al.*, "Semi-Empirical Gibbs Free Energy Formulations for Minerals and Fluids for the Use in Thermodynamic Databases of Petrological Interest," Phys. Chem. Miner. **31**, 1–27 (2004).
38. T. V. Gerya, K. K. Podlesskii, and L. L. Perchuk, "Data Base and Program GEOPATH of Mineral Thermobarometry," in *Experimental Mineralogy: Some Results at the Century Threshold* (Nauka, Moscow, 2004), pp. 188–208 [in Russian].
39. T. V. Gerya, L. L. Perchuk, D. D. van Reenen, *et al.*, "Two-Dimensional Numerical Modeling of Pressure–Temperature–Time Paths for the Exhumation of Some Granulite Facies Terrains in the Precambrian," J. Geodynam. **30** (1–2), 17–35 (2000).
40. T. V. Gerya, L. L. Perchuk, W. V. Maresch, *et al.*, "Thermal Regime and Gravitational Instability of Multi-Layered Continental Crust: Implications for the Buoyant Exhumation of High-Grade Metamorphic Rocks," Eur. J. Mineral. **14**, 687–699 (2002).
41. S. L. Harley, "An Experimental Study of Partitioning of Fe and Mg Between Garnet and Orthopyroxene," Contrib. Mineral. Petrol. **86** (4), 359–373 (1984).
42. S. L. Harley, "The Origin of Granulites: a Metamorphic Perspective," Geol. Mag. **126**, 215–231 (1989).
43. R. J. Hart, D. E. Moser, and M. A. G. Adreoli, "Archean Age for the Granulite Facies Metamorphism Near the Center of the Vredefort Structure, South Africa," Geology **27**, 1091–1094 (1999).
44. R. J. Hart, I. McDonald, M. Tredoux, *et al.*, "New PGE and Re/Os Isotope Data from Lower Crustal Sections of the Vredefort Dome and a Reinterpretation of Its "Crust on Edge Profile," S. Afr. J. Geol. **107**, 83–94 (2004).
45. K. Hisada, L. L. Perchuk, T. V. Gerya, *et al.*, "*P–T* Fluid Evolution in the Mahalapye Complex, Limpopo High-Grade Terrane, Eastern Botswana," J. Metamorph. Geol. **23**, 313–334 (2005).
46. A. Hofmann, A. Kröner, and G. Brandl, "Field Relationships of Mid- to Late Archaean High-Grade Gneisses of Igneous and Sedimentary Parentage in the Sand River, Central Zone of the Limpopo Belt, South Africa," S. Afr. J. Geol. **101**, 185–200 (1998).
47. T. J. B. Holland and R. Powell, "Internally Consistent Thermodynamic Data Set for Phases of Petrological Interest," J. Metamorph. Geol. **16**, 309–343 (1998).
48. L. Holzer, R. Frey, J. M. Barton, *et al.*, "Unraveling the Record of Successive High-Grade Event in the Central Zone of the Limpopo Belt Using Pb Single Phase Dating of Metamorphic Minerals," Precambrian Res. **87**, 87–115 (1998).
49. D. E. James, M. J. Fouch, and J. C. van Decar, "Tectonospheric Structure Beneath Southern Africa," Geophys. Res. Lett. **28** (13), 2485–2488 (2001).
50. S. L. Kamo, W. U. Reimold, I. E. Krogh, *et al.*, "A 2.023 Ga Age for the Vredefort Impact Event and a First Report of Shock Metamorphosed Zircons in Pseudotachylitic Breccia and Granophyre," Earth Planet. Sci. Lett. **144**, 369–388 (1996).
51. M. Yu. Koreshkova, L. K. Levskii, and V. V. Ivannikov, "Petrology of a Lower Crustal Xenolith Suite from Dikes and Explosion Pipes of the Kandalaksha Graben," Petrologiya **9** (1), 89–106 (2001) [Petrology **9** (1), 79 (2001)].
52. S. P. Korikovsky and L. L. Perchuk, "Systematic Variations of the *P–T* Parameters of Regional Metamorphism: Evidence from Microprobe Mineral Study," Izv. Akad. Nauk SSSR, Ser. Geol., No. 5, 79–90 (1983).
53. S. P. Korikovsky, *Metamorphic Facies of Metapelites* (Nauka, Moscow, 1979) [in Russian].
54. S. P. Korikovsky, *Metamorphism, Granitization, and Postmagmatic Processes in the Precambrian of the Udokan–Stanovoi Zone* (Nauka, Moscow, 1967) [in Russian].
55. D. S. Korzhinskii, *Selected Works. Metamorphic Petrology* (Nauka, Moscow, 1999) [in Russian].
56. K. Kreissig, L. Holze, R. Frei, *et al.*, "Geochronology of the Hout River Shear Zone and the Metamorphism in the Southern Marginal Zone of the Limpopo Belt, Southern Africa," Precambrian Res. **109**, 145–173 (2001).
57. A. Kröner, P. Jaeckel, A. Hofmann, *et al.*, "Field Relationships and Age of Supracrustal Beit Bridge Complex and Associated Granitoid Gneisses in the Central Zone of the Limpopo Belt, South Africa," S. Afr. J. Geol. **101**, 201–213 (1998).
58. A. Kröner, P. Jaeckel, G. Brandl, *et al.*, "Single Zircon Ages for Granitoid Gneisses in the Central Zone of the Limpopo Belt, Southern Africa, and Geodynamic Significance," Precambrian Res. **93**, 299–337 (1999).
59. I. N. Krylov, I. M. Gorokhov, E. P. Kutyavin, *et al.*, "Dating of Polymetamorphic Rocks of the Sharyzhalgai Group, Southwestern Baikal Area," in *Geochronology of Eastern Siberia and Russian Far East* (Nauka, Moscow, 1980), pp. 80–94 [in Russian].
60. *Metamorphic Zoning and Polymetamorphic Complexes* (Nauka, Moscow, 1983) [in Russian].
61. M. V. Mints, V. N. Glaznev, A. N. Konilov, *et al.*, *Early Precambrian of Northeastern Baltic Shield: Paleogeodynamics, Structure, and Evolution of the Continental Crust* (Nauchnyi Mir, Moscow, 1996) [in Russian].
62. D. E. Moser, R. M. Flowers, and R. J. Hart, "Birth of the Kaapvaal Tectosphere 3.08 Billion Years Ago," Science **291**, 465–468 (2001).

63. T. Nguiri, J. Gore, and D. E. James, "Crustal Structure beneath Southern Africa and Its Application for the Formation and Evolution of the Kaapvaal and Zimbabwe Cratons," Geophys. Res. Lett. **28** (13), 2501–2504 (2001).
64. C. W. Passchier and R. A. Trouw, *Microtectonics* (Springer, Berlin, 1996).
65. L. L. Perchuk and A. V. Krotov, "Petrology of the Mica Schists of the Tanaelv Belt in the Southern Tectonic Framing of the Lapland Granulite Complex," Petrologiya **6** (2), 165–196 (1998) [Petrology **6** (2), 149 (1998)].
66. L. L. Perchuk and I. V. Lavrent'eva, "Experimental Investigation of Exchange Equilibria in the System Cordierite–Garnet–Biotite," Adv. Phys. Geochem. **3**, 199–239 (1983).
67. L. L. Perchuk and I. V. Lavrent'eva, "Experimental Study of Mineral Equilibria in the System Garnet–Orthopyroxene–Amphibole," Int. Geol. Rev., No. 5, 486–507 (1990).
68. L. L. Perchuk and T. V. Gerya, "Buoyant Ascent of Granulite Complexes: I. Geological–Petrological Test," in *Experimental and Theoretical Simulation of Mineral Formation* (Nauka, Moscow, 2004), pp. 137–157 [in Russian].
69. L. L. Perchuk, "Gas–Mineral Equilibria and Possible Geochemical Model of the Earth's Interiors," Phys. Earth Planet. Inter. **13**, 232–239 (1976).
70. L. L. Perchuk, "Configuration of *P–T* Trajectories as a Record of High-Temperature Polymetamorphism", Dokl. Akad. Nauk **401** (2), 217–220 (2005) [Trans. Russ. Acad. Sci., Earth Sci. Sec. **401** (2), 311 (2005].
71. L. L. Perchuk, "Metamorphic Evolution of Shields and Fold Belts," Geol. Carpathica **36**, 179–189 (1985).
72. L. L. Perchuk, "The Course of Metamorphism," Int. Geol. Rev. **28**, 1377–1400 (1987).
73. L. L. Perchuk, "*P–T* Fluid Regimes of Metamorphism and Related Magmatism with Specific Reference to the Granulite-Facies Sharyzhalgay Complex of Lake Baikal," in *Evolution of Metamorphic Belts*, Ed. by S. Daly, B. W. D. Yardley, and R. A. Cliff, Geol. Soc. London Spec. Publ. **2** (20), pp. 275–291 (1989).
74. L. L. Perchuk, *Thermodynamic Regime of Deep-Seated Petrogenesis* (Nauka, Moscow, 1973) [in Russian].
75. L. L. Perchuk, "Thermodynamic Control of Metamorphic Processes," *Energetics of Geological Processes*, Ed. by S. K. Saxena and S. Bhattacharji (Springer, New York, 1977), pp. 285–352.
76. L. L. Perchuk, D. A. Tokarev, D. D. van Reenen, *et al.*, "Dynamic and Thermal History of the Vredefort Explosion Structure in the Kaapvaal Craton, South Africa," Petrologiya **10** (5), 451–492 (2002) [Petrology **10** (5), 395 (2002)].
77. L. L. Perchuk, L. Ya. Aranovich, K. K. Podlesskii, *et al.*, "Precambrian Granulites of the Aldan Shield, Eastern Siberia, USSR," J. Metamorph. Geol. **3**, 265–310 (1985).
78. L. L. Perchuk, T. V. Gerya, D. D. van Reenen, *et al.*, "The Limpopo Metamorphic Belt, South Africa: 2. Decompression and Cooling Regimes of Granulites and Adjacent Rocks of the Kaapvaal Craton," Petrologiya **4** (6), 619–648 (1996) [Petrology **4** (6), 571 (1996)].
79. L. L. Perchuk, T. V. Gerya, D. D. van Reenen, *et al.*, "Formation and Dynamics of Granulite Complexes within Cratons," Gondwana Res. **4** (4), 729–732 (2001a).
80. L. L. Perchuk, T. V. Gerya, D. D. van Reenen, *et al.*, "Geodynamic Interpretation of the Diversity of *P–T* Paths from Different Portions of the Same High-Grade Terrain," Gondwana Res. **4** (4), 732–734 (2001b).
81. A. L. Perchuk, V. O. Yapaskurt, and S. K. Podlesskii, "Genesis and Exhumation Dynamics of Eclogites in the Kokchetav Massif near Mount Sulu-Tyube, Kazakhstan," Geokhimiya, No. 10, 979–988 (1998) [Geochem. Int. **10**, 877 (1998)].
82. A. L. Perchuk, Doctoral Dissertation in Geology and Mineralogy (IGEM, Moscow, 2003).
83. Z. I. Petrova and V. I. Levitskii, *Petrology and Geochemistry of Granulite Complexes of the Baikal Region* (Nauka, Novosibirsk, 1984) [in Russian].
84. Z. I. Petrova, V. I. Levitskii, V. I. Smirnova, *et al.*, "Geochronology of the Sharyzhalgai Group, Southern Baikal Region," in *Geochronology of Eastern Siberia and Russian Far East* (Nauka, Moscow, 1980), pp. 95–100 [in Russian].
85. M. Raith and P. Raase, "High Grade Metamorphism in the Granulite Belt of Finnish Lapland," J. Geol. Soc. Spec. Publ. London **24**, 283–295 (1986).
86. M. Schaller, O. Steiner, and I. Studer, "Exhumation of Limpopo Central Zone Granulites and Dextral Continent-Scale Transcurrent Movement at 2.0 Ga Along the Palala Shear Zone, Northern Province, South Africa," Precambrian Res. **96**, 263–298 (1999).
87. W. Schreyer, "Subduction of Continental Crust to Mantle Depths: Petrological Evidence," Episodes **11**, 97–104 (1988).
88. C. A. Smit and D. D. van Reenen, "Deep Crustal Shear Zones, High-Grade Tectonites and Associated Alteration in the Limpopo Belt, South Africa: Implication for Deep Crustal Processes," J. Geol. **105**, 37–57 (1997).
89. C. A. Smit, D. D. van Reenen, T. V. Gerya, *et al.*, "*P–T* Conditions of Decompression of the Limpopo High Grade Terrane: Record from Shear Zones," J. Metamorph. Geol. **19**, 249–268 (2001).
90. F. S. Spear and F. P. Florence, "Thermobarometry in Granulites: Pitfalls and New Approaches," Precambrian Res. **55**, 209–241 (1992).
91. F. S. Spear, *Metamorphic Phase Equilibria and Pressure–Temperature–Time Paths* (Mineral. Soc. Am., Washington, DC, 1993).
92. Z. V. Spetsius and V. P. Serenko, *Composition of Continental Upper Mantle and Lower Crust of the Siberian Platform* (Nauka, Moscow, 1990) [in Russian].
93. G. Stevens, R. L. Gibson, and G. T. R. Droop, "Mid-Crustal Granulite Facies Metamorphism in the Central Kaapvaal Craton: the Bushveld Complex Connection," Precambrian Res. **82**, 113–132 (1997).
94. A. A. Tomilenko and V. P. Chupin, *Study of Fluid Inclusions in Metamorphic Complexes* (Nauka, Novosibirsk, 1983) [in Russian].
95. J. L. R. Touret and T. H. D. Hartel, "Synmetamorphic Fluid Inclusions in Granulites," in *Granulites and Crustal Evolution*, Ed. by D. Vielzeuf and Ph. Vidal (Kluwer, New York, 1990), pp. 397–417.

96. J. L. R. Touret, "Fluids in Metamorphic Rocks," Lithos **55**, 1–25 (2001).

97. P. J. Treloar, M. J. Coward, and B. W. Harris, "Hymalayan–Tibetian Analogies for the Evolution of the Zimbabwe Craton and Limpopo Belt," Precambrian Res. **55**, 571–587 (1992).

98. N. G. Udovkina, *Eclogites of the Polar Urals* (Nauka, Moscow, 1972) [in Russian].

99. D. D. van Reenen, C. Roering, and G. Brandl, "The Granulite Facies Rocks of the Limpopo Belt, Southern Africa," in *Granulites and Crustal Evolution,* Ed. by D. Vielzeuf and Ph. Vidal (Kluwer, Dordrecht, 1990), pp. 257–289.

100. D. D. van Reenen, D. Roering, and L. D. Ashwal, "The Archaean Limpopo Granulite Belt: Tectonics and Deep Crustal Processes," Precambrian Res. **5** (1992).

101. D. D. van Reenen, L. L. Perchuk, C. A. Smit, *et al.*, "Structural and *P–T* Evolution of a Major Cross Fold in the Central Zone of the Limpopo High-Grade Terrain, South Africa," J. Petrol. **45**, 1413–1439 (2004).

102. D. D. van Reenen and C. A. Smit, "The Limpopo Metamorphic Belt, South Africa: 1. Geological Setting and Relationship of the Granulite Complex with the Kaapvaal and Zimbabwe Cratons," Petrologiya **4** (6), 610–618 (1996) [Petrology **4** (6), 562 (1996)].

103. C. J. J. Wei, R. Powell, and L. F. Zhang, "Eclogites from the South Tianshan, NW China: Petrological Characteristics and Calculated Mineral Equilibria in the Na_2O–CaO–FeO–MgO–Al_2O_3–SiO_2–H_2O System," J. Metamorph. Geol. **21**, 163–181 (2003).

104. A. Zeh, R. Klemd, S. Buhlmann, *et al.*, "Pro- and Retrograde *P–T* Evolution of Granulites of the Beit Bridge Complex (Limpopo Belt, South Africa): Constraints from Quantitative Phase Diagrams and Geotectonic Implications," J. Metamorph. Geol. **22**, 79–95 (2004).